

**Mercury Spatial and Temporal Distribution in Bottom
Sediments from Kagoshima Bay: Influence of
Submarine Hydrothermal Activity and Relationship
with Physical and Chemical Factors.**

Wilder Leonardo Gamboa Ruiz

March 2015

Abstract

Kagoshima Bay is located on the south coast of Kyushu Island, Japan. Submarine fumaroles present in the northern might be a natural source of mercury in the bay.

This research is part of a broader investigation into the environmental assessment of mercury in Kagoshima Bay. The aim of the present work is to study the horizontal and vertical distributions of mercury in the bottom sediments of the bay and their relationship with major physicochemical properties that might affect the transport of mercury in the ecosystem surrounding this area. Sediment core samples were collected in the north and central areas in surveys performed during 2011 and 2014. The individual core samples were sliced and processed for the analysis of total mercury (T-Hg), chemical composition, total organic carbon (TOC), particle size and magnetic susceptibility (MS).

The horizontal distribution of mercury indicates that fumaroles are the primary source of Hg in the area; also, bottom features were found to possibly affect the dispersion of Hg. The results suggest that mercury is associated predominantly with TOC in the northern part of the bay, indicating a key role of organic matter binding to the Hg. In the area to the west of the fumaroles, the relationship between Hg and TOC is characterized by two linear trends that correspond to the upper and lower sections of the cores. From the physicochemical properties it was suggested that the two distinct linear relations might be caused by a change of the volcanic activity at the Aira Caldera, which is located at the northern part of the bay. The extent of the bay impacted by the Hg generated from the hydrothermal vents has decreased in recent years and is limited to the vicinity of the emission point.

Keywords

Total mercury, organic matter, marine sediment, hydrothermal vents, Kagoshima Bay

List of Figures

Figure 1. Global cycle of Mercury. The width of the arrows is proportional to the importance of the fluxes.	7
Figure 2. Map of Kagoshima Bay showing the sampling sites and the craters Minamidake and Showa in the Sakurajima Volcano..	14
Figure 3. Scheme of the CVAAS and reduction systems.....	17
Figure 4. Representation of the CIELab color space.....	20
Figure 5. Horizontal distribution of the studied physicochemical parameters at Kagoshima Bay..	24
Figure 6. Correlation between the average values of the TOC and the particle size distribution.....	26
Figure 7. Vertical profiles of particles larger than 2 mm found by sieving analysis.....	28
Figure 8. CIE L*a*b* color horizontal distribution of sediments.....	30
Figure 9. X-Ray images and magnetic susceptibility profiles.....	32
Figure 10. Vertical Distribution of T-Hg and TOC for the stations 10, 7 and 2 obtained at different samplings.	34
Figure 11. Vertical distribution of the total mercury concentration and total organic carbon.	36
Figure 12. Scatter plots of TOC vs T-Hg	38
Figure 13. Vertical distribution of the magnetic susceptibility	42
Figure 14. Correlation between T-Hg and TOC concentrations in the bottom sediments in the central area of Kagoshima Bay.....	44

Contents

1. Introduction	5
1.1 Mercury in the Environment	5
1.2 Toxicology of Mercury	8
1.3 Mercury in Kagoshima and Human Health Concerns	9
1.4 Objectives	10
2. Methodology	12
2.1. General description of Kagoshima Bay	12
2.2. Sampling	12
2.2.1. <i>Sample Collection and Pre-treatment</i>	15
2.3. Analytical Procedures	16
2.3.1. <i>Total Mercury (CVAAS)</i>	16
2.3.2. <i>Elemental Composition (WD-XRF)</i>	18
2.3.3. <i>Total Organic Carbon</i>	18
2.3.4. <i>Particle Size Distribution (LD)</i>	18
2.3.5. <i>Color (CIELab Color Space)</i>	19
2.3.6. <i>Magnetic Susceptibility</i>	20
2.3.7. <i>X-Radiograph</i>	20
3. Results and Discussion	22
3.1. Physicochemical properties of the sediments	22
3.1.1. <i>Elemental Composition</i>	22
3.1.2. <i>Particle Size</i>	24
3.1.3. <i>Total Organic Carbon</i>	28
3.1.4. <i>Color</i>	29
3.1.5. <i>Magnetic Susceptibility</i>	31
3.1.6. <i>X Radiograph</i>	31
3.2. Spatial Distribution of Mercury	32
3.3. Relationship between Mercury and physicochemical properties of the sediments	34
4. Conclusions	45

1. Introduction

1.1 Mercury in the Environment

Nowadays, environmental degradation generated by anthropogenic activities is one of the main challenges humanity is facing. Among the harmful effects on the biophysical environment, pollution by toxic metals is an issue that has received great attention due to its impact. Despite of the abundant evidence linking the harmful effects of toxic metals to humans and other organisms (Athar and Ahmad 2002; Gallego et al. 1996; Graeme and Pollack 1998) and their strong environmental impact since they are cumulative and non-biodegradable, exposure continues because of the lack of both environmentally friendly practices and concrete prevention policies (Kim et al. 2014; Liu et al. 2014; Hahladakis et al. 2013; Xu et al. 2013).

Within the group of toxic metals, Mercury (Hg) is one of the most dangerous environmental pollutants and has been recognized as a potential environmental and public health threat by scientist and governments. It is widely considered as one of the pollutants which causes more concern and receives a high global priority because it is present in a diversity of chemical and physical forms with a wide variety of properties that determine its complex distribution, bioconcentration and acute toxicity. Additionally, exposure to mercury even in small amounts, is a great danger to humans and wildlife; for this reason it can constitute a hazard even in environments that are apparently unpolluted. It has been included in several guidelines as one of the most noxious pollutants in every environmental compartments (EU, 2000; WHO, 2000).

Mercury exists in three oxidation states: Hg° (elemental), Hg^{+} (mercurous) and Hg^{2+} (mercuric) mercury. The latter forms a variety of inorganic as well as organometallic compounds. In the case of organometallic derivatives, the mercury atom is covalently bound to one or two carbon atoms. Mercury is emitted to the atmosphere by several processes including natural degassing of the earth's surface and by reevaporation of mercury vapor previously deposited on the earth's surface, in the form of elemental vapor (Hg°).

Although all the species of mercury are toxic, the effects are closely related to its chemical form. The most environmentally interesting species are elemental mercury (Hg°), inorganic Hg (Hg^{2+}), monomethylmercury (CH_3Hg^+ , MeHg^+), monoethylmercury ($\text{CH}_3\text{CH}_2\text{Hg}^+$, EtHg^+) and dimethylmercury (CH_3HgCH_3 , DMeHg). In the biogeochemical cycle of Hg, these species may be transformed into each other and dynamically transported through the terrestrial, aquatic and atmospheric environmental compartments. The most relevant process mercury undergoes in the environment is the transformation of inorganic mercury into methylmercury by bacterial activity and the subsequent accumulation through the aquatic food chain attaining its highest concentrations in large predatory species at the top of the aquatic food-chain. This is the most common way it enters to the human diet. This situation leads to the mercury bioconcentration by hundred or thousand fold causing a potential human and ecological impact (Keating et al., 1997).

Chemical substances undergo cycling and transformations in the environment, and this also the case for mercury. Mercury exists in different physical states and chemical forms at commonly encountered physicochemical conditions, and is susceptible to undergo biological transformations, therefore it is subject to complex and difficult to predict changes in concentration and form.

Human activities constitute an important source of Hg, releasing a significant proportion of the total amount entering the atmosphere each year (UNEP, 2013). These sources include emissions from coal-burning power plants, waste incineration, chlorine production and artisanal gold mining (Pacyna et al., 2010). Furthermore, mercury is released to the environment by natural processes like weathering of Hg-containing rocks, as well as volcanic and geothermal activities (Pyle and Mather, 2003; Varekamp and Buseck, 1986).

Mercury is released into the environment from both natural processes and human activities. Once it has entered the environment mercury cycles between air, land and water bodies until it is eventually removed by sedimentary processes. It and can either stay close to the source for long periods, or distribute on a regional or even global basis. Mercury is widely distributed in the atmosphere since is its high volatility one the main important factors affecting the biogeochemical cycle of this element.

In the atmosphere, where approximately 95% of total mercury is in the elemental state, it is slowly oxidized to the mercuric state. Hg^0 can circulate in the atmosphere for up to a year, and hence can be widely dispersed and transported thousands of miles from sources of emission. As a result, while the principal emissions of mercury are from punctual sources concentrated in industrial regions, mercury pollution is global. The return of mercury from the atmosphere to the Earth's surface occurs mainly via wet precipitation of dissolved Hg^{2+} (see figure 1) (More et al., 1998). Once oxidized, around 60% of atmospheric mercury is deposited to land and 40% to water, even though land represents only 30% of the Earth's surface (More et al., 1998). In oceanic waters, after it undergoes a complex set of chemical and biological transformations, most of the Hg^{2+} is reduced to Hg^0 and returned to the atmosphere; only a small fraction is permanently exported to the sediments. Inorganic mercury can be methylated to mono- and dimethylmercury. Laboratory and field studies have shown the methylation of Hg^{2+} mainly by micro-organisms.

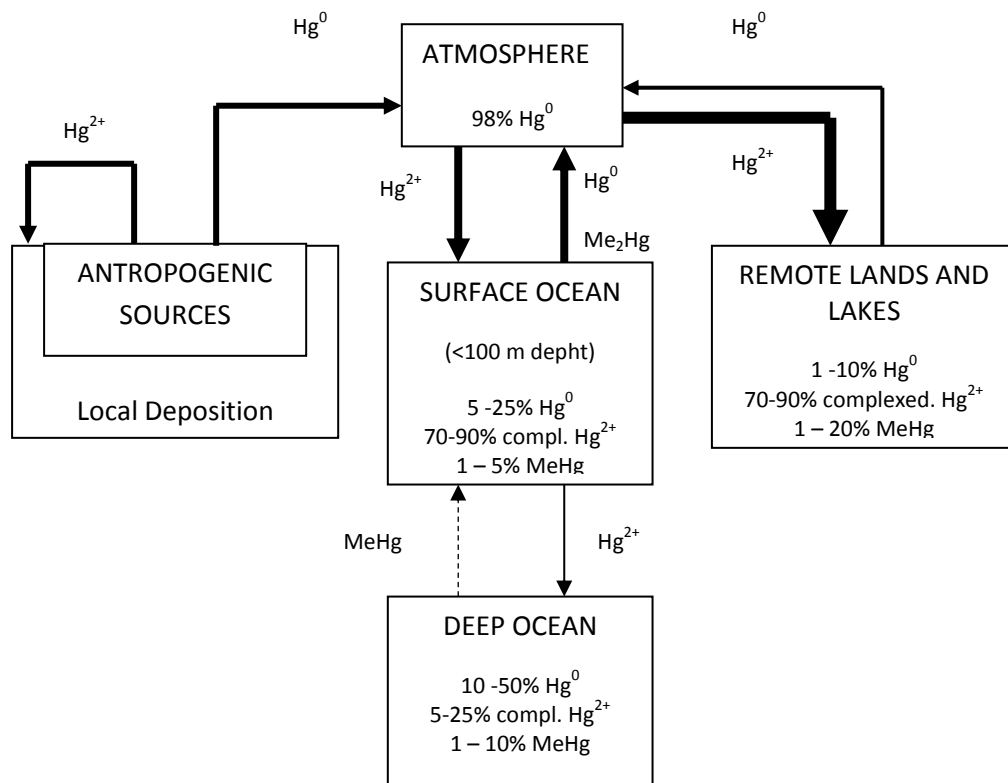


Figure 1. Global cycle of Mercury. The width of the arrows is proportional to the importance of the fluxes. (Adapted from More et al, 1998)

Levels of methylmercury in waters are usually much lower than those of inorganic mercury. This is due to the difficulty of methylation reactions in aqueous phases, from one side, and to the easy decomposition by solar UV light of organomercury compounds from the other. In sediments and biota the levels of methylmercury are higher than in waters because of accumulative phenomena.

Soils and sediments constitute concentrated reservoirs of trace metals in which the amounts are higher than those present in other environmental compartments, such as water. The concentrated pollutants can be potentially released due to changes in the physicochemical conditions, for this reason a key factor in the assessment of environmental risk is the evaluation of the concentration of the metals distribution among the different phases of these solid matrices (Liu et al. 2014; Xu et al. 2013). Taking into account the high affinity of the inorganic mercury for sulfides, it is logical to expect that this strong binding controls the chemistry of mercury in sediments and anoxic waters.

1.2 Toxicology of Mercury

Mercury has a unique volatility among the elements. This makes it quite mobile in the environment. This mobility is further enhanced because it can be methylated biologically (primarily by aquatic bacteria). Methylated Hg has special chemical characteristics (due to the methyl group) that make it prone to bioaccumulate in animals and plants; in contrast, inorganic Hg does not bioaccumulate. Methylmercury is considerably more toxic than elemental mercury and its inorganic salts, because it is efficiently adsorbed from the gastrointestinal tract due to its lyphophilicity, it is rapidly transported through biological membranes and accumulates on the surface of nerve cells causing neuronal damage (Sweet et al, 2001).

The generally recognized adverse effects attributed to the Hg exposure include stomatitis, erethism, and renal damage (for oral exposure). Toxic responses, such as axial malformations, stunting, neurological deficits, decreased of weight, altered enzyme levels, and renal failure, are examples of chemically induced effects of Hg exposure (Graeme and Pollack 1998). Targets of inorganic mercury include proteins, which bind mercuric ions to sulfhydryl groups resulting in structural and catalytic protein alteration. Inorganic mercury is a central nervous system and renal toxicant. In

contrast, methyl mercury is well-absorbed across membranes and is efficiently accumulated by biota. The primary target of methyl mercury toxicity is the central nervous system. Methyl mercury accumulates in muscle tissue where it binds to sulfhydryl groups of muscle proteins (WHO, 2000)

1.3 Mercury in Kagoshima and Human Health Concerns

Kagoshima is the largest city southern of Kyushu, with a population of 600,000 people. The city is located in an area with high volcanic activity and several volcanoes are in the vicinity, including Sakurajima, an active volcano located across Kagoshima Bay. The bay is the main source of marine resources in the region; for this reason, alarm was raised when a survey conducted in 1973 revealed that 10 out of 14 fish species captured in the bay exceeded the provisional control limit of 0.4 mg/kg total mercury (Kagoshima Prefecture, 1975). These results prompted the establishment of projects aimed at identifying the mercury source, and subsequent surveys revealed that submarine fumaroles present at the northeastern area of the bay release mercury (Osaka et al., 1976). Furthermore, the mercury concentration has been monitored in environmental samples and biota. Higher Hg levels have been found near the fumaroles in seawater samples (Ando et al., 2010; Sakamoto, 1993). Sediment samples have been studied as well, and high levels of mercury were found near the area where the fumaroles are located (Sakamoto et al. 1985; Sakamoto et al., 1995; Tomiyasu et al., 2007).

Although there is no current evidence of current environmental pollution caused by submarine hydrothermal vents, further understanding of the mercury behavior in the area is of great interest to protect the people consuming seafood from these waters. The studies performed to date suggest that mercury released from the fumaroles is predominantly immobilized in the sediments, but there is not enough information regarding the spatial distribution of mercury. Moreover little is known about the link between the Hg distribution and the physicochemical properties of the sediments, and a satisfactory explanation has yet to be proposed regarding the mechanism involved in the bio-concentration of mercury found in biota in 1973.

1.4 Objectives

Research has shown that mercury can be a threat to the health of people and wildlife even in environments that are not obviously polluted. The risk is determined by the likelihood of exposure, the form of mercury present (some forms are more toxic than others), as well as the geochemical and ecological factors that influence how mercury moves and changes form in the environment. For this reason it is important to understand the behavior of mercury emitted by hydrothermal activities in the northern area of the bay even if currently these activities do not pose an imminent risk.

In the present thesis, the horizontal and vertical distributions of mercury in the sediments of Kagoshima Bay were determined to gain insight into the influence of the fumarolic activity on the transport of Hg in the area, because sediments can be used to obtain information regarding historical changes in the concentration that may not be readily apparent using samples collected from the water column. In addition, to identify the main properties of the sediments that might affect the transport of Hg in this area, some of the physicochemical properties of the sediments, including elemental composition, organic matter content, particle size, magnetic susceptibility, color and sedimentary structures were determined.

Submarine hydrothermal vents represent an important source of Hg in marine environments and often develop at high depths in remote areas, such as mid-ocean ridge spreading centers. The presence of shallow hydrothermal activity offers a valuable opportunity to understand the factors affecting the dispersion of mercury emitted from this type of natural sources.

The objectives of this research are:

- a) Investigate the horizontal and vertical distributions of total mercury in bottom sediments from Kagoshima Bay in order to estimate the impact of the hydrothermal vents located in the north-eastern area of the bay.
- b) Determine the relationship between the observed mercury distribution and some physicochemical properties of the sediments, to identify the main factors affecting the transport of the emitted mercury.

- c) Estimate the potential environmental risk associated with the emission of mercury, using its spatial distribution, historical variations and relationship with the properties of this marine environment.

2. Methodology

2.1. General description of Kagoshima Bay

Kagoshima Bay is located in the central part of the Kagoshima Prefecture, which extends from 30° 59'N to 32° 11'N and from 130° 06'E to 131° 12'E and constitutes the southern portion of Kyushu Island (Figure 2). Kagoshima Prefecture is divided Bay into three areas by the Kagoshima: the Hokusatsu area in the north, the Satsuma Peninsula in the southwest and the Ōsumi Peninsula in the southeast. The bay is located between the Satsuma and Ōsumi peninsulas and has an elongated shape, opening southwards with a length of approximately 75 km has a width of approximately 25 km. The bay contains submarine calderas and four active volcanoes (i.e. Wakamiko, Sakurajima, Ikeda and Kaimondake). Taking into account the topographical features of the bay, it can be divided in three main basins: bay head, central area and bay mouth. The volcano Sakurajima is currently active, and its effects on the Hg concentration in the atmosphere of Kagoshima city are continuously monitored (Tomiyasu et al., 2000; Tomiyasu et al., 2006; Miyamoto et al., 2008; Kono and Tomiyasu, 2014). The volcano is connected to the east side of the Ōsumi Peninsula and is located between the bay head and the central areas, which are joined only through a narrow (~ 3.5 km) and shallow (~ 40 m) passage. Notably, this passage inhibits the circulation of water between the two areas (Oki, 1989). The bay head area has a semi-circular shape and corresponds to the Aira caldera, which is a gigantic volcanic caldera created by a massive eruption approximately 22,000 years ago (Arakami, 1984). The topography of the western portion of the bay head is rather flat, with a depth of 140 m, whereas the eastern portion has complex features. There, the deepest part (~ 200 m) corresponds to a small basin called Wakamiko crater (4 km × 2 km), where the active submarine fumaroles are located. The depth decreases to approximately 70 m towards the west of the Wakamiko caldera. The central area constitutes the widest portion of the bay and has a basin shape with a depth that increases steadily to a maximum of approximately 230 m (Hayasaka et al, 1976).

2.2. Sampling

Bottom sediment samples were collected within the bay head and central areas at 14 different points as displayed in Figure 2. In the bay head area, sediments were collected

from 10 sampling points, 4 were located in the east side (Stations 2S, 2, 9 and 8) and 6 in the west side (Stations 7, 6, 5, 7N, 6N and 5N). Sampling points were selected taking into consideration the area topography and the main external sediment sources. Station 2 is located in Wakamiko caldera, the deepest area of bay head (approximately 200 m), close to the active hydrothermal vents. Stations 2, 9 and 8 form a straight line pointing to the northwest, the bottom profile among these stations increases smoothly from 200 m at stations 2 and 8, to 150 m at St. 9. Amori River is the main watercourse in the area and flows into the northern Kagoshima Bay (42.5 km long with a drainage area of 411 km² and an average flow of 21 m³s⁻¹) (Kagoshima Prefecture, 2008; Cho et al. 1991; Tsutsumi et al. 2009) The placement of stations 9, 8 and 2 was selected to allow the evaluation of the sediment load carried by the river as the flow leaves the mouth. At the west of the Wakamiko caldera lays wide area with uniform features, with a depth of approximately 150 m, stations 7, 6 and 5, 7N, 6N and 5N are located in this area. Stations 7, 6 and 5, are arranged in a straight line at the west of station 2. The change in the bottom depth with respect to Station 2 is pronounced, allowing the chance to estimate the influence of the bays head topography on Hg dispersion. Stations 7N, 6N and 5N are located at the north of stations 7, 6 and 5, respectively; these stations are located at similar depth but closer to the shore.

In the central area, sediments were collected at 4 points (Stations 10, 11, 12, and 13) arranged in a straight line from the west Sakurajima passage to the center of the bay. Depth increases gradually from station 10 to station 13 (150 m to 250 m, respectively) allowing the comparison of the impact of hydrothermal fluids with a water body isolated from the emission point. Several sampling activities were performed between February of 2011 and June of 2013; the dates and the parameters measured at each survey are described in Table 1.

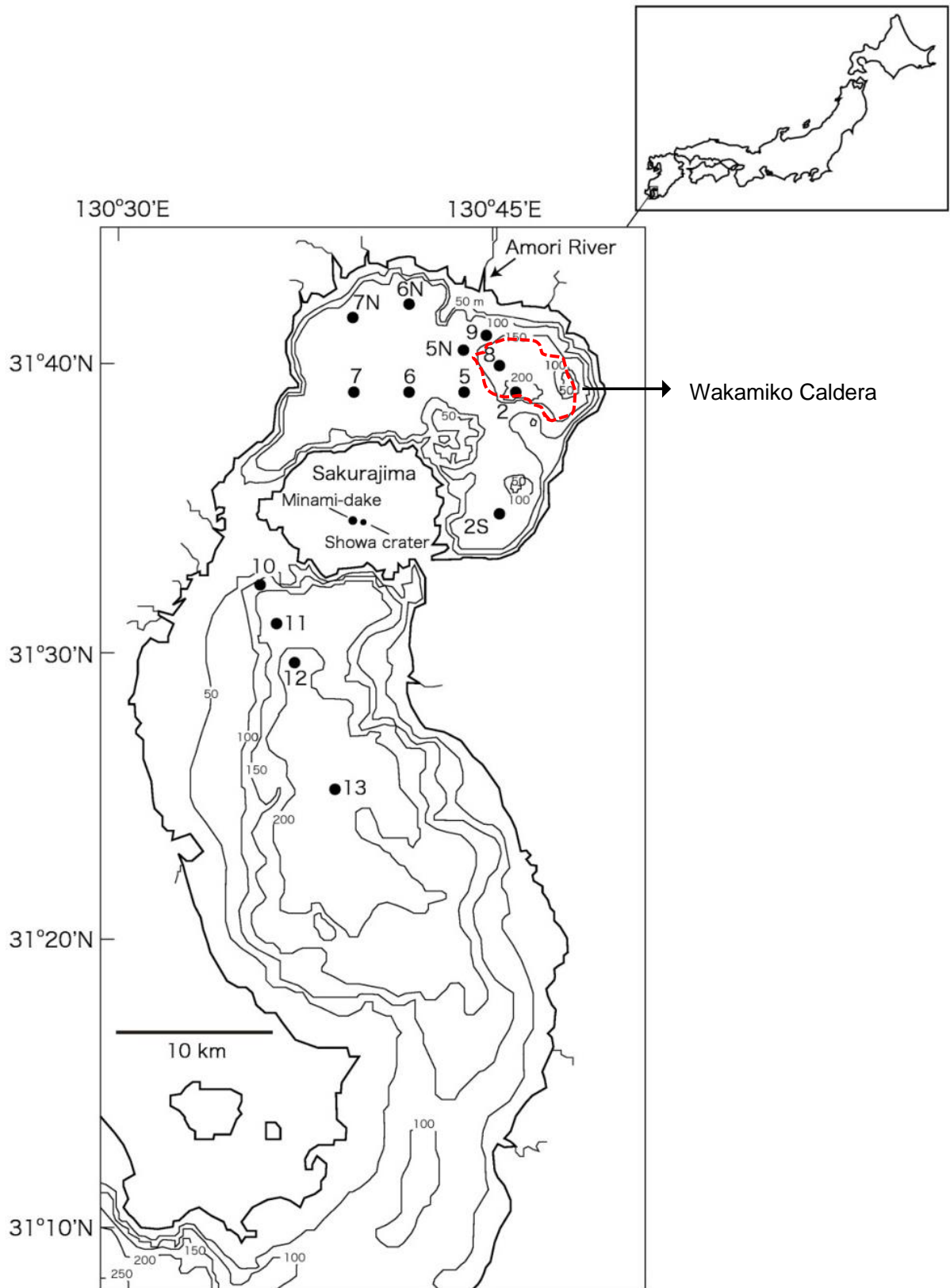


Figure 2. Map of Kagoshima Bay showing the sampling sites and the craters Minami-dake and Showa in the Sakurajima Volcano. Minami-dake presented periods of heightened activity during the 1970s and 1980s, Showa crater has been active since 2006.

Table 1. Sampling activities performed in Kagoshima Bay. T-Hg: Total mercury, TOC: Total organic carbon, EC: Elemental composition, PSD: Particle size distribution, M.S: Magnetic susceptibility.

Date	Station													
	2	8	9	7	6	5	10	11	12	13	7N	6N	5N	2S
2011.2.28	T-Hg													
	TOC													
	E.C.													
2011.5.19	T-Hg													
	TOC													
	E.C.													
2011.8.26	T-Hg													
	TOC													
	E.C.													
2011.12.1	T-Hg													
	TOC													
	E.C.													
	M.S.													
2012.10.9							T-Hg							
							TOC							
							E.C.							
							PSD							
							M.S.							
2012.12.3							E.C.							
							T-Hg							
							TOC							
							E.C.							
2013.2.4	PSD										T-Hg			
											TOC			
											E.C.			
							PSD				PSD			
							M.S.				M.S.			
2013.6.6											T-Hg			
											TOC			
											E.C.			
							PSD				PSD			
							M.S.				M.S.		M.S.	

2.2.1. Sample Collection and Pre-treatment

Bottom sediments were collected using a gravity corer; the retrieved cores were approximately 40 cm long. The cores were sliced at intervals of 2 cm, packed and sealed in polyethylene bags, and then transported immediately to the laboratory. The samples were homogenized, and a portion of each sample was dried at 40 °C. Pumice fragments were found at several stations comprising diverse core depths. After the fragments were excluded, sediments were ground to a fine powder using an agate mortar. The last time the volcanic activity of Sakurajima developed into an eruption,

that was accompanied by a massive ejection of pumice was during the Taisho eruption in 1914; therefore, sediments deposited simultaneously with the pumice date after this event.

2.3. Analytical Procedures

2.3.1. Total Mercury (CVAAS)

The determination of total mercury (T-Hg) in the sediment samples was performed by cold vapor atomic absorption spectrometry (CVAAS), using a well-established method based on the proposed by the Japanese Ministry of the Environment (Ministry of Environment 2004, Akagi 1985, Akagi et al. 1995) that has been validated through inter-laboratory exercises (Malm et al., 1995). In this method, the sediment samples are subjected to wet digestion on a hot plate leading to the oxidation of the different mercury species to the mercuric ion (Hg^{2+}). The next step involves the reduction of the Hg^{2+} to elemental mercury (Hg^0) with tin chloride (SnCl_2) followed by the introduction of the elemental mercury to the detection system where the absorption is measured at 253.7 nm.

This methodology uses a circulation-open air flow system presented in figure 3 (Mercury analysis manual, 2004). In this system elemental mercury is generated in the reaction vessel by the addition of 10% SnCl_2 and circulated via a 4-way valve at a flow rate of 1 – 1.5 L/min for 30 seconds in order to homogenize the gas phase, during this step the gas is bubbled into an acidic gas trap containing NaOH 5N. Subsequently, the valve is rotated 90° and then the humidity is removed in a moisture trap consisting of an ice bath; after, the gas is pumped into the photo-absorption cell and released into the atmosphere after retaining the mercury in a solution of KMnO_4 0.5% in H_2SO_4 0.5 M

A portion of dried sediment (0.1 g) was placed into a 50 mL volumetric flask; next, 1 mL of deionized water flask were swirled to ensure complete wetting of the sample, 2 mL of a 1:1 mixture of conc. HNO_3 : HClO_4 and 5 mL of conc. H_2SO_4 were added. The flasks were heated on a hot plate for 20 min at 230 °C. Finally, the flasks were allowed to cool, brought to volume with ultra-pure water and analyzed using a CVAAS (Semiautomatic Analyzer HG-3000, Sanso Seisakusho Co., Ltd., Japan).

Mercury was measured by adding fixed volumes of the sample solutions into the reaction vessel of the mercury analyzer (maximum 10 mL). Elemental mercury vapor

(Hg⁰) was generated by adding 1 mL of SnCl₂ 10% in HCl previously bubbled with N₂ during 20 minutes. Instrument response was registered with a chart recorder (SS 250F Recorder. Sekonic. Tokyo, Japan).

The calibration curve was made using a stock solution of 0.1 mg/kg Hg in H₂SO₄ 0.05 M prepared from a 1000 mg/kg HgCl₂ standard solution (ultra-pure grade, brand). Since T-Hg concentration is measured as a function of peak height, a calibration curve of peak height versus the amount of T-Hg must be constructed. For each batch of samples, two blanks as well as four calibration standards were prepared by adding fixed volumes of the stock solution (usually 25, 50, 75 and 100 µL) with a micropipette; the weight of the added standard was registered and used for the construction of the calibration curve instead of the volume. Blanks and standards were treated with the same digestion procedures as the samples. Accuracy control was performed using the marine sediment reference material CRM 7302-a (T-Hg: 0.52 ± 0.03 mg/kg), prepared by the Metrology Management Center, National Institute of Advanced Industrial Science and Technology (AIST), Japan. Determinations were performed in duplicate and each digested sample was measured two times. Blanks were prepared and no appreciable Hg contamination was detected.

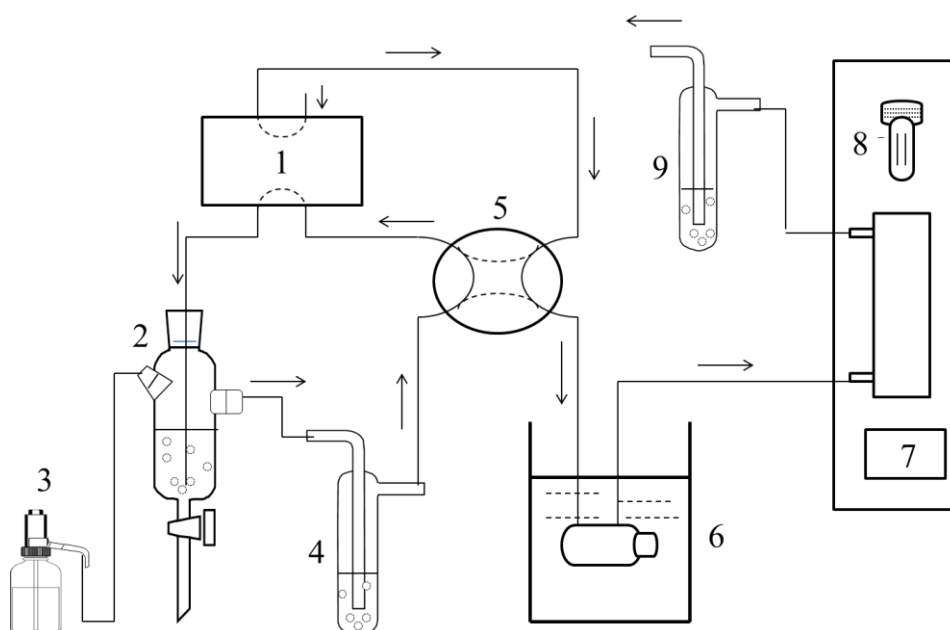


Figure 3. Scheme of the CVAAS and reduction systems. 1: Air pump. 2: Reaction vessel. 3: Tin chloride dispenser. 4: Acidic gases trap (5N NaOH). 5: 4-way valve. 6: Moisture Trap (ice bath). 7: Detector. 8: Hg lamp. 9: Hg trap (1% KMnO₄). Adapted from Mercury analysis manual, 2004.

2.3.2. *Elemental Composition (WD-XRF)*

Elemental composition (EC) was analyzed by the Wavelength Dispersive X-Ray Diffraction Fluorescence technique (WD-XRF) (SZX-mini II, Rigaku Co., Ltd., Japan), which is a non-destructive method for the quantification of the mayor elements.

In this technique, the elements in the sample are excited by irradiation with high energy X-rays. Each element emits secondary x-rays at characteristic wavelengths. The resulting fluorescent X-rays are collimated and then diffracted by an analytical crystal. When X-rays encounter the analytical crystal at a specific angle Θ , only those X-rays that satisfy Bragg's law are reflected and a single wavelength reaches the detector. Consequently, by placing the analytical crystal different angles, a wide range of wavelengths can be scanned. Since each element has characteristic emission wavelengths, secondary X-rays from one element at a time can be measured on the spectrometer. This equipment Calibration of the equipment was carried out with a pulse height adjustment (PHA) standard.

2.3.3. *Total Organic Carbon*

Total Organic Carbon (TOC) was determined as the difference between Total Carbon (TC) and Inorganic Carbon (IC) using a total carbon analyzer TOC-V SCN (Shimadzu Co., Ltd., Japan) attached to a solid sample module SSM-5000A (Shimadzu Co., Ltd., Japan). For the determination of TC, 50 mg of sediment was carefully weighted in a ceramic boat, introduced to the instrument and finally combusted at 980 °C. IC was determined on 50 mg of sample by adding 1 mL of H₃PO₄ 1:1 and subsequent heating at 240 °C.

2.3.4. *Particle Size Distribution (LD)*

Particle size distribution of the sediments was determined by the laser diffraction (LD) technique with a SALD-3100 measurement system (Shimadzu Co., Ltd., Kyoto, Japan). A few grams of wet sediment were taken from each sample and sieved retaining the particles larger than 2 mm. The obtained suspension was allowed to deposit and after 48 hours the overlying water was carefully extracted with a syringe and discarded. The deposited fraction was re-suspended with about 25 mL of deionized water and transferred to polyethylene bags, then samples were thoroughly mixed and a portion of was used for the particle size distribution measurements.

The measurement system is composed of two units: a dispersing bath and the measuring unit. When a sample is introduced into the dispersing bath, it is dispersed by the action of an ultrasound homogenizer and a stirrer. The suspension is then circulated through the measurement unit by a pump and the measurement starts after the concentration of the suspended material reaches a fixed concentration. When the analysis is finished, the suspension is discharged and the system is washed with deionized water until the detected signal decreases to the background level.

The Shimadzu SALD-3100 has the capacity to handle samples with grain sizes ranging from 0.05 μm to 3000 μm . The particles in the analyzed samples were classified into 51 size ranges from 0.05 to 2000 μm . Results were obtained as spectra of fractions, median values and weight averages.

During the first step of the particle size distribution analysis, samples are screened retaining fragments larger than 2 mm (ϕ : -1). These fragments were carefully washed, and then the number, size and types of particles retained were recorded.

2.3.5. *Color (CIELab Color Space)*

Color measurements were performed using a handled color reader SPAD-503 (Konika Minolta, Japan) operating with a tungsten lamp and a sample illumination angle of 8° (viewing geometry 8/D). During a measurement, samples are illuminated and the reflected wavelengths are filtered, detected and transformed into numeric values with the CIE 1976 (L*a*b) color space (or CIELab). This color space is comparable to the way human visual system interprets color in the framework of the opponent process color theory, which conceives the perceived information about color as the proper combination of three independent stimuli (Hurvichi et al., 1957). CIELab translates color stimuli into distinctions between light and dark, red and green, and blue and yellow; these values are indicated with three axes: L* (lightness), a* (red/green) and b* (yellow/blue). In the Figure 4, the central axis represents lightness (L*) whose values run from 0 (black) to 100 (white). Color axes are based on the fact that a color cannot be both red and green or blue and yellow because these colors oppose each other. In these axes, values run from negative to positive. On the a* axis, a color stimuli in the +a direction depicts a shift towards red. Along the b* axis, +b movement represents a shift towards yellow. At the center of both color axes the color is neutral gray. In this way, sample color is interpreted as the combination of three numeric values.

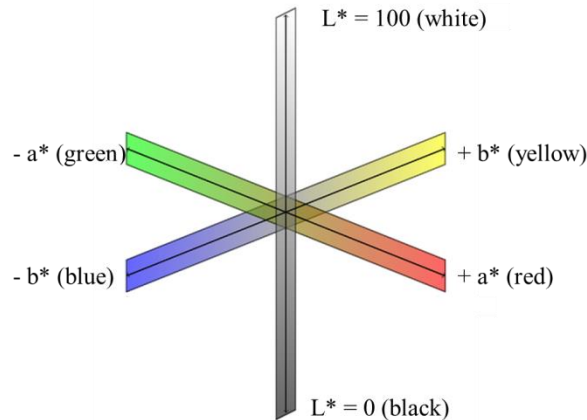


Figure 4. Representation of the CIELab color space

Measurements were performed placing the color reader on the sample perpendicularly. Dried samples were analyzed taking the average of three measurements after adjusting the reader with a white colored calibration plate.

2.3.6. *Magnetic Susceptibility*

Magnetic Susceptibility is the degree to which a material can be magnetized in the presence of an external magnetic field. Magnetic susceptibility analysis was performed using a handheld magnetic susceptibility meter KT-10 (Terraplus Inc., Canada). This instrument uses a 10 kHz oscillator with an inductive coil to generate a magnetic field. The analysis is performed by measuring the difference in frequency and amplitude of the oscillator when the instrument is operated in free air and on the sample. The change in the oscillator is proportional to the extent of the sample magnetization.

There are three steps in the measurement sequence: the first is a free air measurement; the second is the sample measurement; and the final step is another free air measurement. Dried samples were measured by triplicate. The results correspond to volume magnetic susceptibility (χ) expressed in SI units.

2.3.7. *X-Radiograph*

The methodology followed to obtain the X-ray images of the cores follows the method outlined by Axelsson (1983). Sediment cores were collected and transported to the lab in vertical position inside the coring tubes. After the overlying water was drained and sediments consolidated, cores were horizontally retrieved from the coring tubes and cut longitudinally in order to obtain samples of regular cross section (approximately 3 cm).

The slice was put inside a soft X-ray unit M-150W (Softex CO, LTD., Kanagawa, Japan) directly under the X-ray tube in horizontal position and then a film sheet was placed under the sediment slice carefully. Subsequently, the sample was irradiated at 75.2 kV and 1.99 mA and the exposed film was developed with an automatic processing machine MR-SE-2 (Max-RHEIN, Japan). The obtained radiographic films were photographed in a dark room using a digital camera and a portable X-ray film viewer.

3. Results and Discussion

3.1. Physicochemical properties of the sediments

3.1.1. Elemental Composition

Changes in the sediments geochemical composition might allow the identification of biogeochemical processes leading to changes in the sediment properties that might affect the interaction with Hg (Lopez et al., 2006)

The elemental composition of the sediments is presented in Table 2. Sediments consist predominantly of silicon and aluminum. These are the main elements associated with the alumino-silicates, that have been identified as the main minerals in the sediments of the area (e.g.. halloysite, kaolinite, illite, smectite and chlorite) (Carranza et al., 1994). High contents of Fe_2O_3 and weak correlation coefficient between $\text{Fe}_2\text{O}_3/\text{SO}_3$ suggest the presence of iron oxyhydroxides.

The elemental composition of the sediments reveals a relatively narrow compositional variation, suggesting that the sediment matrix does not significantly change along the bay. No significant correlation between the main components of the sediments was found (Table 3); therefore, no noticeable trends were distinguished when comparing the behavior of the most abundant components. In addition, correlation analyses were performed using different data subsets (e.g.. only stations located in the central part of the bay or stations from the northern area were considered). However, no significant correlations were found for these datasets either. Nevertheless, some tendencies were found for the distribution of calcium, as shown in Figure 5a. The calcium concentration follows the pH of the overlying water among the different stations. The average concentration of Ca (expressed as CaO) ranged from 3.07 to 9.03 %, reaching the lowest calcium concentration near the fumaroles, where the pH of the overlying water was at its lowest value (pH= 6.86 at St.2), whereas the highest concentration was measured in the central part of the bay (pH of approximately 8). As seen in Table 2, the sulfur concentration (expressed as SO_3) ranged from 0.92 to 3.17 %, with the maximum concentration near the fumaroles. The increase in sulfur content in the sediments is likely caused by the effect of the sulfide compounds contained in the hydrothermal fluids. The horizontal distribution of Ca and sulfur indicates that the impact of the hydrothermal activity is limited to the northern portion of the bay. Therefore,

considering the influence of the submarine fumaroles, the area can be divided into two main zones: a hot spot in the north and a relatively unaffected region in the central basin, which can be considered as the background.

Table 2. Elemental compositions of the studied sediments. The reported values correspond to the mean of the core sample. Superscripts a and b correspond to the highest and lowest values in each column, respectively.

Station	Na ₂ O	MgO	Al ₂ O ₃	SiO ₂	P ₂ O ₅	SO ₃	Cl	K ₂ O	CaO	TiO ₂	MnO	Fe ₂ O ₃
13	3.13	2.43	13.71 ^a	59.59 ^a	0.98	1.27	2.92 ^b	2.25	8.72 ^b	0.79	0.59	6.14
12	3.13	2.69 ^b	13.92	60.12	0.94	1.11	2.60	2.19	7.77	0.73 ^a	0.58	6.06 ^a
11	2.93	2.54	14.23	59.95	0.97	1.10	2.26	2.27	7.84	0.84	0.44	6.45
10	2.72 ^a	1.89	14.63	59.73	0.98	1.20	1.63	2.29	7.83	0.91	0.21	7.53
7	3.41	2.46	14.32	59.34	0.96	0.98	2.55	2.29	6.15	0.86	0.90 ^b	7.68
6	3.19	2.09	14.04	60.29	0.95	0.95	2.19	2.45	6.26	1.00 ^b	0.59	8.30 ^b
5	3.20	1.87	14.34	61.51	0.95	0.98	2.05	2.37	5.75	0.93	0.23	7.79
7N	3.13	1.96	15.32	60.57	0.93 ^a	1.29	2.75	2.25	4.68	0.85	0.65	7.17
6N	3.01	1.85	16.12	62.31 ^b	0.94	1.17	2.15	2.34	4.34	0.73	0.27	6.80
5N	3.14	1.56 ^a	16.88	60.90	0.97	1.43	2.26	2.29	4.19	0.83	0.16	6.90
9	3.15	1.60	17.88 ^b	59.77	1.13 ^b	2.00	2.57	2.84 ^b	3.07 ^a	0.87	0.34	7.32
8	3.51 ^b	1.60	16.34	60.16	1.09	3.17 ^b	2.86	2.66	3.34	0.78	0.47	7.19
2	2.92	1.75	14.28	61.82	0.98	2.92	2.57	2.35	4.59	0.84	0.15 ^a	7.18
2S	3.53	1.92	15.07	59.22	0.94	0.92 ^a	1.61 ^a	2.12 ^a	6.90	0.93	0.28	7.57

Table 3. Correlations between the main components of the sediments.

	Na ₂ O	MgO	Al ₂ O ₃	SiO ₂	P ₂ O ₅	SO ₃	Cl	K ₂ O	CaO	TiO ₂	MnO	Fe ₂ O ₃
Na ₂ O	1											
MgO	-0.063	1										
Al ₂ O ₃	0.174	-0.742	1									
SiO ₂	-0.350	-0.388	0.127	1								
P ₂ O ₅	0.171	-0.466	0.628	-0.223	1							
SO ₃	0.075	-0.531	0.378	0.226	0.672	1						
Cl	0.175	0.167	0.058	0.007	0.332	0.480	1					
K ₂ O	0.130	-0.530	0.640	0.043	0.891	0.574	0.323	1				
CaO	-0.240	0.788	-0.806	-0.456	-0.511	-0.599	-0.250	-0.674	1			
TiO ₂	0.060	-0.186	-0.153	-0.243	-0.064	-0.288	-0.538	0.070	0.098	1		
MnO	0.378	0.654	-0.350	-0.494	-0.128	-0.263	0.511	-0.086	0.256	-0.084	1	
Fe ₂ O ₃	0.257	-0.420	0.068	-0.021	0.056	-0.060	-0.438	0.271	-0.285	0.829	-0.034	1

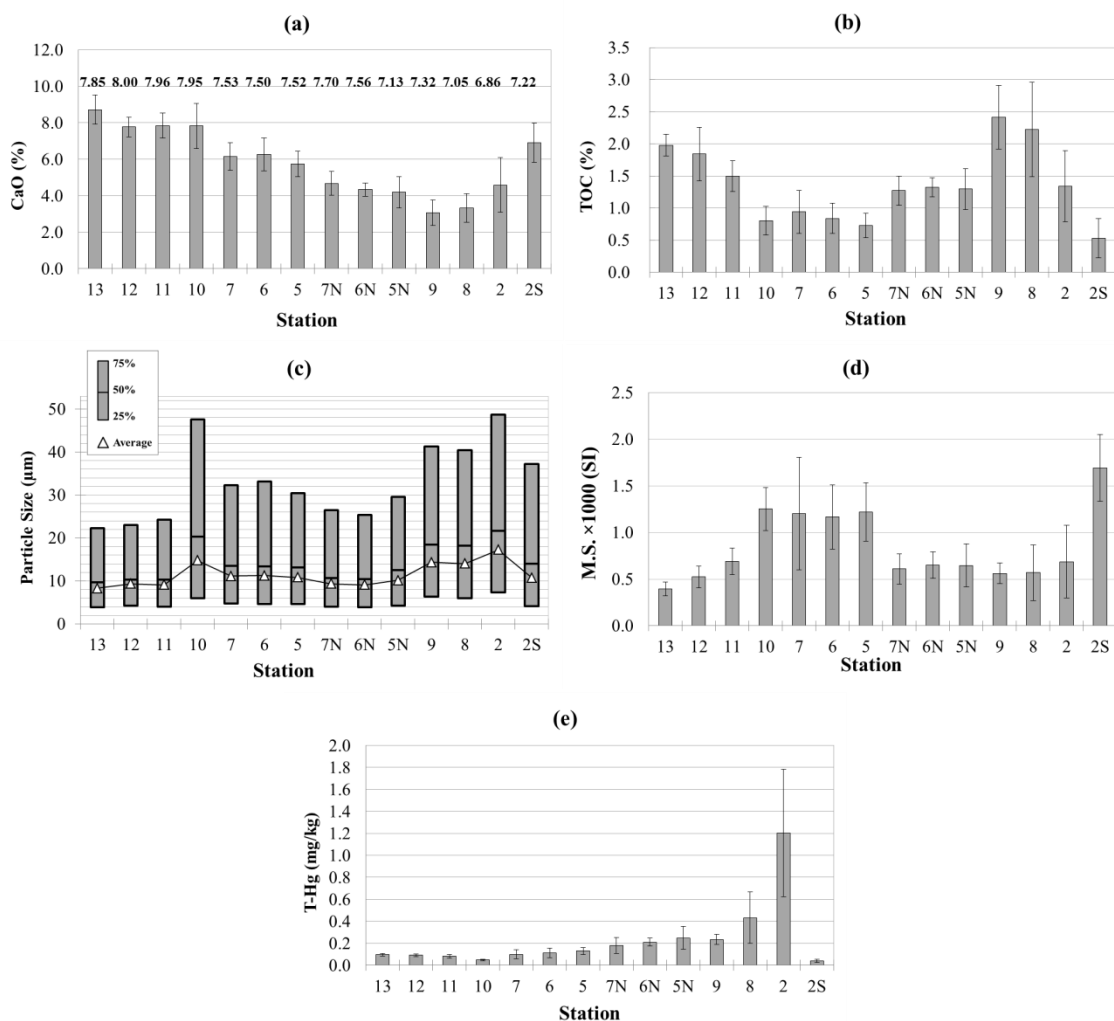


Figure 5. Horizontal distribution of the studied physicochemical parameters at Kagoshima Bay. a) Total calcium (g-CaO/100-g) and the pH of the overlying water, b) total organic carbon (g/100-g), c) particle size distribution (μm), d) magnetic susceptibility (SI), and e) total mercury (mg/kg). The error bars correspond to the standard deviation.

3.1.2. Particle Size

Particle size is the most fundamental physical property of sediment. Information on grain size can be used to study trends in surface processes related to the dynamic conditions of transportation and deposition; in environmental studies grain size is a powerful tool to understand the affinities of fine-grained particles and contaminants (Hunerlach et al. 2004). Therefore, with these reasons in mind, the purpose of a grain-size analysis was to accurately determine the frequency distribution, and to calculate a statistical description that adequately characterizes the sample.

The horizontal distribution of particle size was obtained using 25%, 50% and 75% cumulative distributions and average values. As shown in Figure 5c, most stations have similar average values and sorting. Bottom sediments of the studied areas can be characterized as being mainly medium silt in both the central (d_{50} , $\phi = 6.3$) and innermost area (d_{50} , $\phi = 5.9$). The locations that might be more influenced by the rivers flowing into the bay possess coarser particles and have a wider range of particle sizes. For example, the effect of Amori River can be observed at stations 9, 8 and 2 in the northern area, which exhibited larger particle sizes than stations 7, 6, 5, 7N, 6N, and 5N.

However, the particle size at the central portion decreases proportionally with the distance from the shore. As it was indicated previously, water flow in this area leads to the deposition of fine grained particles in the vicinity of station 13. Moreover, station 10 is located at the narrow west Sakurajima passage, which forms a 50 m deep canal. This area is characterized by elevated flow rates; therefore, sea water flowing counterclockwise from the deep central area collides in this narrow region, depositing coarse-grained materials (Oki 1989). High flow rates in this passage are present as a consequence of the construction of breakwaters during the early 1990s, which affected the natural course of the water. Presently, water coming from the central area is being directed toward the narrow path between the coastal structures and the volcano. Water exchange between the two areas is restricted, but the water flow at the passage is high. As a consequence, when the particle size distribution at St.10 is compared with those of the other stations in the central area, it is clear that the sediments at St. 10 are coarser and less sorted.

When the horizontal distribution was considered, an inverse relationship was observed between particle size and the TOC for most of the sampling points (Figure 6), suggesting that the smaller the particle size, the higher the concentration of organic matter of the sediment. The cores at St. 9, 8, 2 and 10 fall outside the linear trend because, as described above, sediments around stations 9, 8 and 2 are affected by the discharge of terrestrial material and St.10 is located at the west Sakurajima passage.

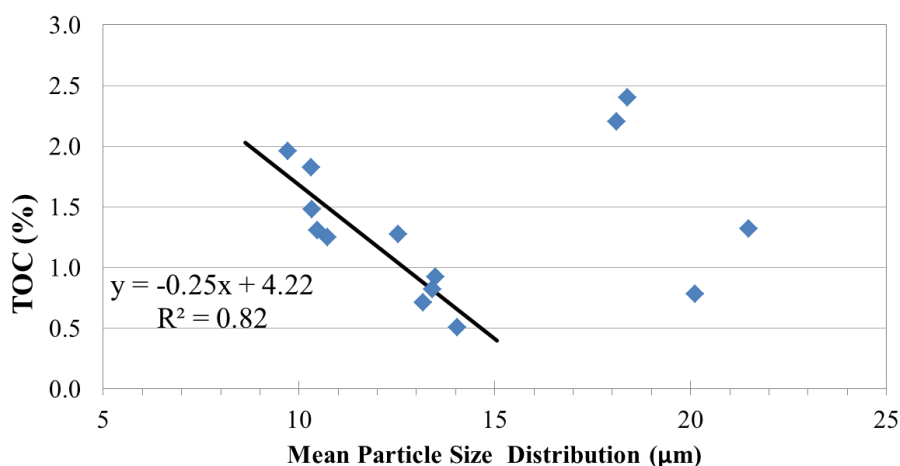


Figure 6. Correlation between the average values of the TOC and the particle size distribution.

The fraction smaller than 2 mm was taken into consideration during the particle size distribution analysis. However, the particles retained (i.e, particle size larger than 2 mm) can also provide useful information. Changes in bottom sediment reflect variations in the hydrological processes taking place in the bay and the proximity and relative importance of sediment sources (Hakanson 1977; Nelson 1983). Vertical changes within sediment cores can provide a record of the evolution of these processes. For this reason, particles larger than 2 mm were carefully removed from the sieve and classified into four main categories: vegetal debris, tephra, pumice and shell fragments. Results presented in figure 7 display changes in sediment sources and physicochemical conditions along the Bay.

Vascular plant debris is abundant at stations 9, 8 and 2, which are located in the vicinity of Amori River, this finding suggests that particulate vegetal detritus that have lived on the land surroundings comprises a primary source of organic matter to the bottom deposits in the northern portion of the Bay head. The input of land-derived material by Amori River was first suggested by the larger particle sizes observed at these stations during particle size distribution analysis. Since organic matter has high affinity with Hg, this finding is probably is important since the Hg emission point is located near this area. Tephra fragments are found at stations 7, 5, 2 and 2S, which are in the proximity of the volcano; this is direct evidence of the influence of the activity of Sakurajima volcano on sediment composition. Volcanic tephra ejected by Sakurajima is deposited predominantly in the surroundings and might have an indirect effect on the binding of

Hg by sediments. Shell fragments are absent near the fumaroles probably as a consequence of the low pH around this area (Figure 5a).

Pumice particles, which are a common product of explosive volcanic eruptions, constitute an exceptional geologic material since its density is often lower than water. Initially, ejected pumice floats on water due to its high porosity, sinking eventually by slow absorption of water into the vesicles. The last volcanic event of Sakurajima accompanied by the ejection of pumice took place during the Taisho eruption in 1914; therefore the presence of pumice offers a chronological reference since sediments buried simultaneously with pumice fragments were deposited after Taisho eruption. It was found that pumice has a wide distribution in sediments of both the central and north basins. In the central basin, the pumice layer gets thicker as the distance from the shore increases (from station 10 to 13). A thick pumice bed comprising most of the sediment column is observed at station 13, probably as a consequence the previously described flow pattern in this area, which favors the deposition of pumice fragments in the midpoint of this basin. Thick pumice beds were also observed in the north basin at 7, 6 and 5; it is clear how the amount and size of the fragments increases with the depth. For instance at station 5, in the 4 to 6 mm layer, one fragment of 3 mm of diameter was observed; on the other hand, from 36 to 38 cm, 216 fragments ranging from 2 to 30 mm were found. This distribution of pumice particles suggests that a single volcanic event generated these pumice beds.

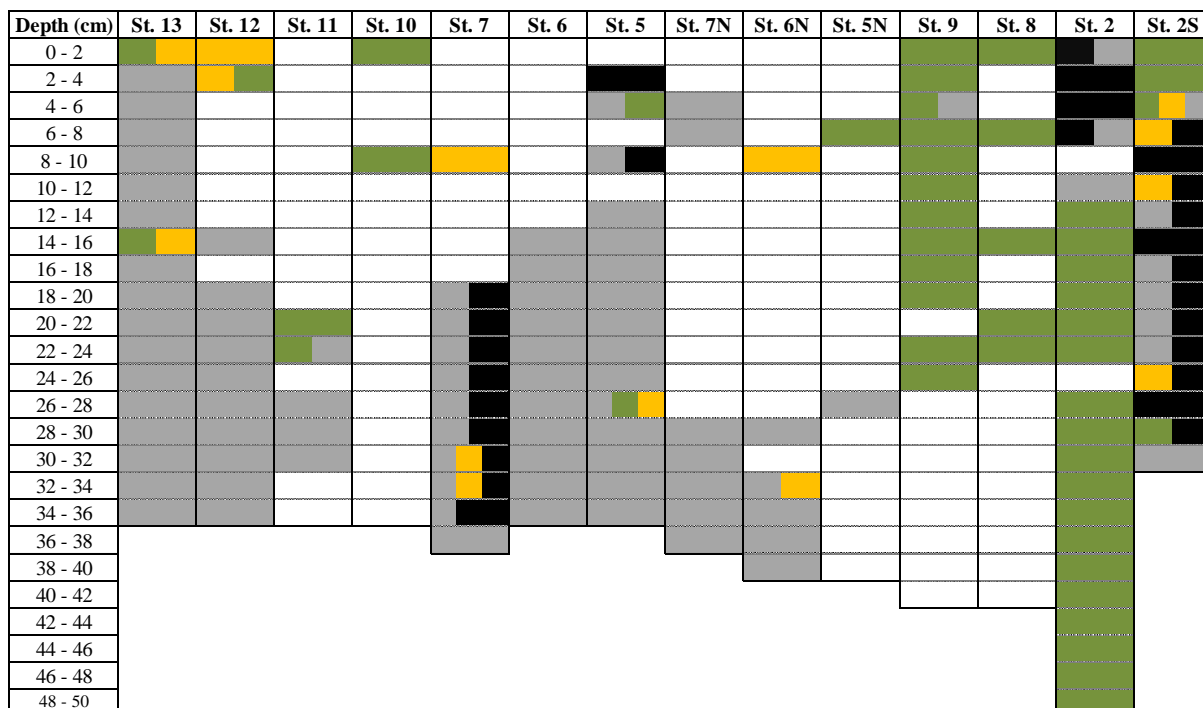


Figure 7. Vertical profiles of particles larger than 2 mm found by sieving analysis. Gray: Pumice. Green: Vegetal debris. Black: Tephra. Yellow: Shell fragments.

3.1.3. Total Organic Carbon

The TOC concentration in the sediments fluctuates widely: for example, the TOC concentration fluctuates from 0.5 ± 0.3 % at St. 2S to 2.4 ± 0.5 % at St. 9 (Figure 5b). Stations 5N, 6N and 7N exhibit similar levels of organic matter, probably because they exist in similar environments and are located at a similar depth and distance from the shore. In the Bay head area, at stations 9, 8 and 2, the TOC concentration decreases with the distance from the coast. This behavior suggests that an important source of organic matter in this area is the Amori River, which is the main inflow river in the north basin and is located towards station 9. Abundant plant debris was found at the stations 9, 8 and 2, providing evidence of the impact of Amori River. Sediments from these locations may contain organic matter of both aquatic and terrestrial origin.

In contrast, an inverse relationship is observed for organic matter contents and depth and distance in the central portion of the bay, the organic matter contents increase as the depth and distance from the shore increase (e.g.. 0.8 ± 0.2 %, 1.5 ± 0.2 %, 1.8 ± 0.4 % and 2.0 ± 0.2 % at stations 10, 11, 12 and 13, respectively). At this region, open-sea water enters through the bay mouth and flows counterclockwise, experiencing a limited exchange with the northern basin because of the barrier constituted by the shallow and

narrow passage connecting both areas. For this reason, fine-grained material circles around the central area and is deposited predominantly at the midpoint of the basin. These fine particles are generally rich in organic matter; therefore, the TOC content increases going from the shore to station 13.

The standard deviation of the TOC at the cores in the central area is considerably lower than that observed at the north. The wider fluctuation of the TOC contents in the north might indicate different sources of organic matter and/or different sedimentation conditions.

3.1.4. Color

Sediment color has always been considered an important qualitative parameter, used as a proxy to describe and distinguish sedimentary characteristics; it is closely related to the sediment composition, which is the product of climate, transport processes and physico-chemical conditions. Color mainly depends on the contents of organic matter, carbonates, quartz and iron, but also on the forms of iron: reddish and yellowish colors are usually associated to ferric (Fe^{3+}) minerals, whereas greenish-grayish colors indicate the presence of ferrous (Fe^{2+}) iron. High organic carbon contents related with anoxic conditions resulting in dark colors, while carbonate is usually related to lightness (Tucker 2003).

Digital measurement of color in sediment samples, which can be acquired with a spectrophotometer through nondestructive manipulation, gives numerical information on the color and is used to describe the sediments as well as to document changes in the depositional conditions (Mix et al. 1992, Debret et al, 2011, Guimaraes et al, 2013). Additionally, this technique is affordable and allows further investigation of the samples afterwards. On such basis, the digital color of the sediments is a parameter considered in the present study as an integrated signal of changes in the mineralogical and chemical composition.

The L^*a^*b values revealed as expected a uniform bulk composition of the bottom sediments from Kagoshima Bay (Figure 8), the horizontal distribution of these values does not change greatly over the different stations and therefore supports the homogeneous mineralogical composition evidenced previously by the elemental composition analysis. Considering the mean values at each station, it can be observed

how sediments have neutral L*a*b* values, being more white than black (L* values from 58.4 to 66.4 at St. 2S and 2, respectively); slightly more red than green (a values from 0.6 to 2.2 at St. 2 and 9) and more yellow than blue (b values from 6.6 to 10.8 at St. 10 and 13).

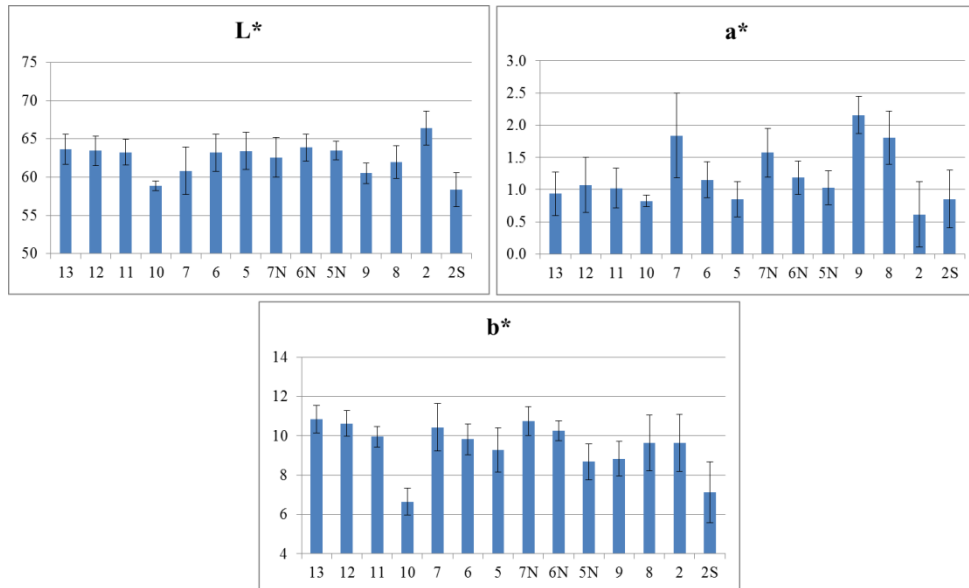


Figure 8. CIE L*a*b* color horizontal distribution of sediments. Results correspond to the mean value and error bars to the standard deviation.

Horizontal profiles of the L*a*b values do not show clear tendencies along the bay; however, there are relationships between the numeric values of the color and the composition of the sediments. L* values show a positive correlation ($r = 0.69$, $P < 0.05$) with SiO₂ concentration, probably because of the association of quartz with the white color of the sediments; on the contrary, organic matter content did not show a negative correlation with L*. Additionally, variations in b* (yellow) data along the different stations suggest an inverse association with Fe₂O₃ ($r = -0.49$, $P < 0.05$).

Vertical distribution of the numerical values of color indicates temporal changes in the sediment bulk composition. Temporal variations in the organic matter concentration correlate with changes in +a* (red) and +b* (yellow) components at most of the stations. Vertical profiles of color constitute a good proxy of changes in sediment mineralogical composition, being associated with fluctuations of organic matter variation in the case of Kagoshima Bay.

3.1.5. *Magnetic Susceptibility*

The horizontal distribution of χ fluctuates between 0.395×10^{-3} and 1.693×10^{-3} SI at St. 13 and 2S, respectively. The horizontal distribution of χ is presented in Figure 5d. As observed, sediments from stations near Sakurajima (St. 10, 7, 6, 5 and 2S) exhibit higher levels of χ than the other stations. The mean values of χ suggest that magnetic minerals are more abundant in the areas near the Sakurajima volcano and that these locations can be strongly affected by volcanic ashes from Sakurajima.

When the horizontal profiles are considered, a statistically significant correlation ($P < 0.05$) arises between χ/Fe ($r^2 = 0.78$), χ/Ti ($r^2 = 0.86$) and χ/TOC ($r^2 = -0.72$). These results corroborate the strong link between the magnetic susceptibility and the presence of paramagnetic materials, such as Fe- and Ti-bearing minerals, as well as their inverse relationship with organic matter. Average values of magnetic susceptibility show an inverse relationship with the color of the sediments as well, a negative relationship with +b* (yellow) was found possibly due to the association of this parameter with the organic matter content.

3.1.6. *X Radiograph*

X-radiographs of sediment cores provide information on the sedimentary fabric of deposits. For example, x-radiographs highlight subtle density differences arising from changes in the depositional environment (Araneda et al, 2007). Samples from stations 7, 5 and 2 were analyzed by this technique.

Images from the three cores present similar features: an area of high reflectance can be clearly observed at the central part. This vertical variation might indicate a higher density of sedimentary structures in this area, probably as a result of the increase in the deposition of mineral particles. This observation is congruent with the vertical profile of magnetic susceptibility since the same portions of the sediment column present an increase in the value of this parameter (Figure 9). This might indicate that in the past, an episodic increase in the deposition of magnetizable minerals, probably volcanic ash, took place affecting the north basin of the Bay. Moreover, vertical profiles of TOC present a decrease in the concentration at the same depths as the areas of high reflectance; this finding further enforces the former hypothesis because an increase of

the proportion of minerals is accompanied by a lessening of the organic matter proportion. This change in the sediment fabric might affect the way Hg interacts with the sediments since organic matter is the main sediment fraction controlling Hg distribution in this area.

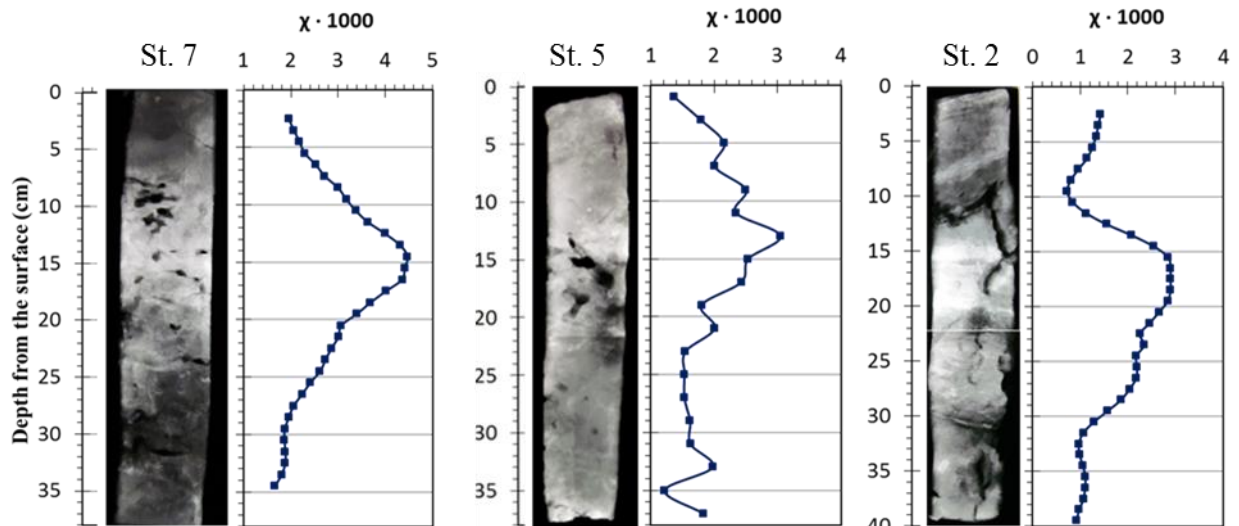


Figure 9. X-Ray images and magnetic susceptibility profiles of cores. from stations 7, 5 and 2.

3.2. Spatial Distribution of Mercury

The average Hg concentration at each station is shown in Figure 5e. The highest total Hg level was found at the station 2 (Average T-Hg: 1.2 mg/kg), where the submarine vents are located. The concentration of T-Hg decreases sharply as the distance from this area increases: 0.23 mg/kg at station 9 and 0.10 mg/kg at station 7.

The spatial distribution of mercury in the bottom sediments is consistent with previous studies (Tomiyasu et al., 2007) and suggests that the bathymetric features of the bay play an important role in the dispersion of the mercury emitted from the fumaroles. The mercury concentration decreases faster towards stations 5, 6 and 7, whereas the drop in the concentration towards stations 8 and 9 is less pronounced. This might be because the bay depth has a gradual slope facilitating the dispersion of mercury in the direction of stations 8 and 9, whereas the slope is steeper toward stations 5, 6 and 7 (Figure 2), which may obstruct the transport of the fluids emitted from the fumaroles. The same behavior is observed in the northwestern area, where the average levels of mercury at stations N7, N6 and N5 are higher than those observed in stations 7, 6, and 5,

suggesting again that the transport of the vent emissions is hindered in locations where the slope of the bay bottom is more steeped. This behavior can also be corroborated by the characteristics of station 2S, where the T-Hg concentration is the lowest among all of the cores (37.6 $\mu\text{g}/\text{kg}$) and the slope in relation to station 2 changes drastically.

The mercury levels found at stations 10, 11, 12 and 13 are low when compared with the northern area, showing that Hg emitted from the hydrothermal vents disperses predominantly in its vicinity. As described above (see Elemental composition), the northern area receives most of the impact from the fumaroles, whereas the central area can be considered as the background of the bay.

The vertical profiles of the T-Hg are shown in Figure 11. Cores from the central area (Stations 10, 11, 12 and 13) do not exhibit significant vertical variations. Because this portion of the bay is not affected by the activity of the fumaroles, major changes in the vertical profile are not observed. The T-Hg levels in the northwestern area (at Stations 7, 6, 5, 7N, 6N, and 5N) decrease markedly towards the surface, and then the concentration becomes rather steady in the layer of approximately 16 to 20 cm. This behavior may indicate that, a progressive decrease in the impact of the hydrothermal activity has occurred in this area.

However, at stations 2, 8 and 9, which are located near the fumaroles, the profile of T-Hg is different compared to what was found in the other areas. For example, the T-Hg level varied widely at station 2 (average $1.2 \pm 0.6 \text{ mg}/\text{kg}$), increasing quickly with depth until the 8-10 cm layer, and then decreasing until the 16-18 cm layer, where the concentration starts increasing again. The vertical variation of T-Hg at this station might be a record of the emissions from the fumaroles and suggests that the source of mercury in the bay is not steady but fluctuates. The profile at station 8 varied widely as well. However, the changes in the concentration are different than those observed at station 2; the Hg levels changed sharply along the core, suggesting different sedimentation regimes between these neighboring stations. At station 9, which is located near the shore, the Hg concentration decreases slightly down-core while oscillating. The vertical distribution of the Hg changes in response to the variations in the hydrothermal activity and to the different sedimentation regimes.

3.3. Relationship between Mercury and physicochemical properties of the sediments

The assessment of the relationship among the different studied variables was performed combining data obtained during the different sampling campaigns, in order to use a large data set. The figure 10 shows the vertical profiles of total mercury and TOC for the stations 2, 7 and 10. When the T-Hg and TOC vertical profiles obtained during different sampling activities are compared, it is observed that for a given station the profiles obtained during different surveys follow similar trends, supporting the reliability of the results since equivalent information can be acquired regardless when the sampling is carried out. This finding is important when combining the data from different samplings to determine the relationship between mercury and the different variables evaluated.

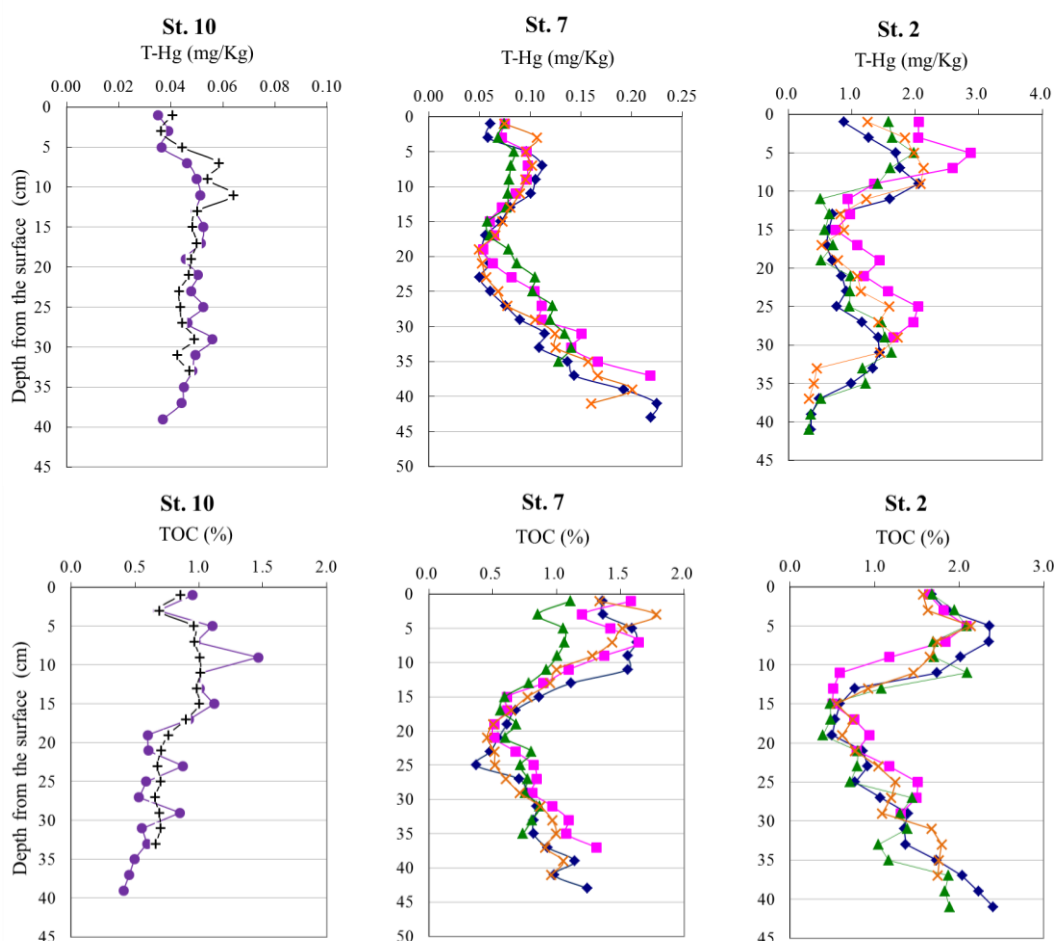


Figure 10. Vertical Distribution of T-Hg and TOC for the stations 10, 7 and 2 obtained at different samplings. (◆: Feb 2011, ■: May 2011, ▲: Aug 2011, ×: December 2011, ●: Oct 2012, + : December 2012)

The relationship between T-Hg and the different variables studied was evaluated and no statistical relationship was found, organic matter was the only parameter that showed a statistically significant relationship with T-Hg and for this reason the discussion in the present section will focus on this variable. Although for most of parameters no direct relationship with T-Hg was observed, their spatial and temporal distribution reveal changes in the depositional environment that further explain the connection between observed T-Hg and TOC distributions.

The ability of organic matter to concentrate mercury has been well recognized; therefore, it is an important factor when evaluating the distribution of Hg in sediments (El Bilali et al., 2002; Sunderland et al., 2006). The TOC exhibited different vertical profiles in Kagoshima Bay. In the central area, the TOC levels decreased down-core and do not appear to be associated with the behavior of T-Hg. However, the TOC vertical distributions mirror the T-Hg at all locations in the northern area, except St. 8, where both parameters exhibit no relationship. The T-Hg and TOC vertical profiles were compared to understand the relationship between these two parameters (Figure 11).

At St.2, the TOC vertical profile mirrors the T-Hg for most of the core, suggesting an association between these two parameters. A similar behavior for the T-Hg and TOC profiles was found at station 2S, although the concentrations of both parameters in this area are rather low (T-Hg: 0.38 ± 0.1 mg/kg, TOC: 0.53 ± 0.36 %). The TOC profile at station 8 varied widely, as did T-Hg, but the changes in the concentration of TOC exhibit no clear relationship with T-Hg. At station 9, both T-Hg and TOC exhibit similar profiles, with a small variation down-core, when compared to their responses at stations 2 and 8. Note that at stations 2, 2S and 9, the T-Hg and TOC profiles behave similarly, but this apparent association is interrupted at station 8, which is located between stations 2 and 9. Station 8 is located near the edge of the Wakamiko caldera, where the depth changes drastically. Therefore, it is possible to consider the wide range of variation of the studied parameters to be a consequence of the erratic supply of material generated by the collapse of the edge of the caldera.

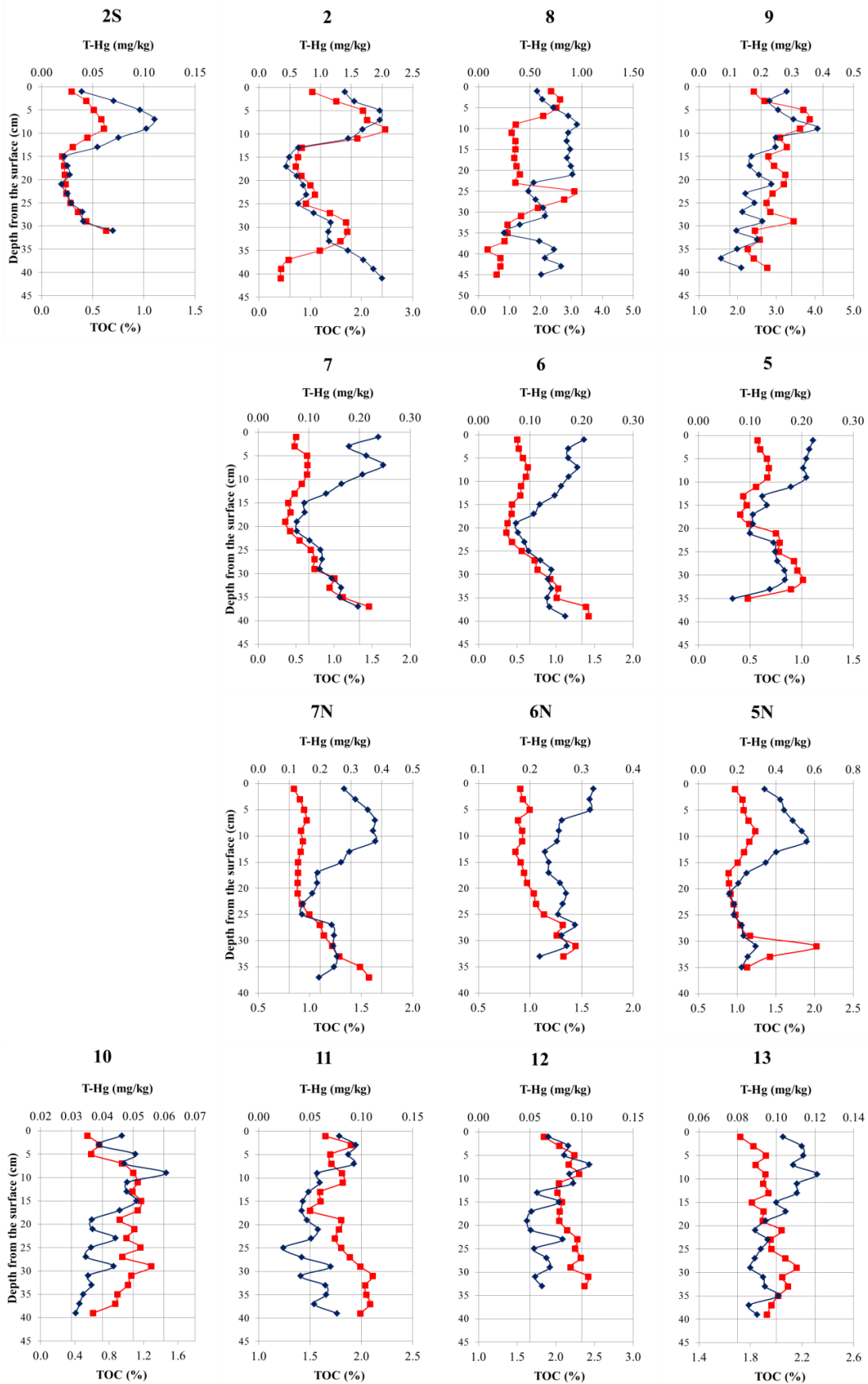


Figure 11. Vertical distribution of the total mercury concentration and total organic carbon. (■:T-Hg (mg/kg), ◆: TOC (g/100-g))

For all of the sampled locations, the vertical profiles of the elemental composition, T-Hg and TOC obtained during different surveys follow similar trends, regardless of the date of the sampling. This finding supports the reliability of the results, which is important when the data from different samplings are combined to determine the relationship between mercury and the other parameters of the sediments.

Linear regression analysis was used to examine whether an association exists between T-Hg and TOC. The results presented in Figure 12 show that there is a positive correlation in some areas of the bay. In the bay head, a statistically significant correlation between the T-Hg and TOC was found ($P < 0.05$) at stations 2, 9 and 2S. In contrast, there is no statistically significant relationship at the station 8 ($r = 0.21$, $n = 86$). The absence of correlation in this station is probably caused by the characteristics of the sedimentation process. At station 2, some outliers from the lower portion of the core were found and removed when calculating the relationship. The strong significant correlations suggest that mercury is bound to the organic matter in the sediment matrix and indicates that organic matter is an important factor in the transport and incorporation of Hg to the sediments in the northern part of the bay.

A different trend emerges when considering the T-Hg and TOC relationship at stations 7, 6, 5, N7, N6 and N5. In this area of the bay, not only one, but two linear relationships are present, suggesting that this section of the northern area has distinct sedimentation conditions. The linear relationships between Hg and TOC found in these stations follow the same behavior. Specifically, the two observed relationships correspond approximately to the upper and lower halves of the cores; in the upper part of the core, the regression has a smaller slope than in the lower part of the core.

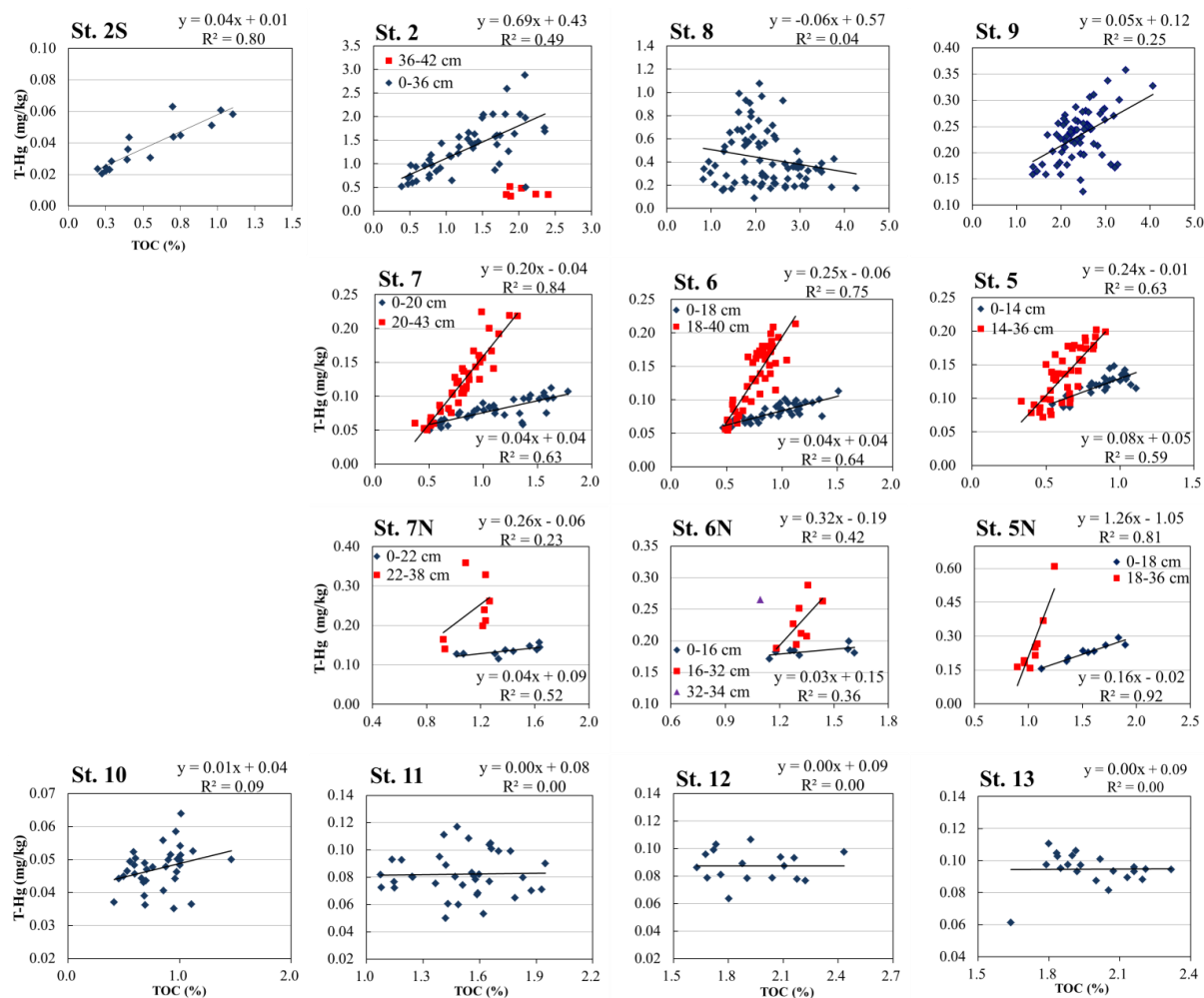


Figure 12. Scatter plots of the total organic carbon (TOC) vs. the total mercury (T-Hg). The solid lines represent the regression lines.

T-Hg and TOC vertical profiles follow the same changes of concentration down-core, but these changes occur at different rates. If the profile of T-Hg were mirrored by TOC for the entire core, then only one linear relationship would be observed; however, this is clearly not the case. When considering the vertical profiles from the bottom to the top of the core, it can be observed how the concentration of both Hg and TOC decrease. However, the TOC content increases markedly up-core near the 16-20 cm layer, whereas T-Hg merely increases. It was found that the vertical profile of the particle size remained uniform for all of the studied locations; thus, no direct connection could be established between this parameter and the vertical changes of TOC and T-Hg. This result indicates that the two linear relationships observed at the northern area are a consequence of other factors not related directly with the particle size.

An up-core increase in the TOC might be partially attributed to an increase of the accumulation rate or an enhanced mobilization of organic matter. Another possible factor that can affect the concentration of organic matter is the dilution by rapid inorganic matter sedimentation. If the sedimentation rate of the inorganic fraction changes with time, an increase in the sedimentation of minerals might lead to a decrease of the organic matter concentration. If, for some reason, the supply of inorganic sediments increases (e.g., because of intensified volcanic activity of Sakurajima), the proportion of mineral components would increase, thereby leading to a decrease of the organic matter proportion.

The vertical profiles of magnetic susceptibility were compared to evaluate the effect of Sakurajima on the sediment composition and to identify areas with similar sedimentation conditions. To evaluate the connection between the observed magnetic susceptibility and the sediment components that most likely influence its value, the vertical distribution of magnetic susceptibility and iron were compared (Figure 13). The magnetic susceptibility profile mirrored the Fe content at station 2, but no similarities were found at the other stations, indicating that χ is not directly related to one main factor for a given sample (i.e., Fe or Ti-bearing materials) but to a combination of several parameters, including paramagnetic and diamagnetic minerals. Common magnetic susceptibility features are observed for the stations 7, 6, 5, 7N, 6N, and 5N. The rock magnetic susceptibility increases smoothly with depth until the 16-22 cm layer is followed by a similarly smooth decrease. This behavior suggests that the sediments present in this area were deposited in comparable depositional environments. These cores also exhibit the two linear relationships between TOC and T-Hg noted previously. The fact that a change in the vertical profile of T-Hg, TOC and χ in the northwestern area occurs in the same layer indicates that an alteration in the sedimentary environment in this area caused a change of the proportion of organic matter in the sediments. In the northern area, a thick pumice layer was found at stations 7, 6 and 5 from the deepest part of the cores until the 18 – 14 cm layer, with the size of the fragments decreasing upwards. If the pumice at the lowest layer of the core was deposited immediately after the year 1914, these cores cover a period of approximately 100 years. The sediment layer where the TOC and T-Hg profiles change and produce the two linear relationships is located around the core center, that is, after the 1960s. This indicates that at

approximately that period of time, the sedimentation conditions changed in this area, resulting in the observed relationships.

Pumice layers can be useful to associate changes in the sedimentation regime with recorded historical events. In order to use this approach, the following assumption has to be made: the pumice layer observed in the sediments at the west of Wakamiko caldera was ejected by Sakurajima volcano in 1914 and its deposition started immediately after the eruption. However, the presence of pumice layers in the sediments can be explained by other mechanisms. For instance, pumice originally deposited on land could have been washed downstream to sink in the Bay with the consequent incorporation of these fragments with a more recent sediment layer. This situation could lead to the wrong identification of these pumice fragments. Tomiyasu et al (2003) studied the vertical profiles of mercury in soils around Sakurajima finding a deposit of Taisho pumice at approximately 1 m from the surface; this observation supports the scenario in which Taisho pumice was ejected by Sakurajima during Taisho eruption and can be found at around 20 cm of depth in the sediments at the north western area of Sakurajima Bay.

A possible cause of the change in the sedimentation conditions can be the emission of ash by the volcano Sakurajima. Between the mid-1970s and the 1980s, the activity of Sakurajima increased markedly at the Minami-dake summit crater. This period was characterized by the emission of large volumes of ash and its subsequent deposition in the surrounding areas. For example, during the year 1985, approximately 16 kg/m² of ash fall was recorded at the local meteorological observatory, which is located 10 km from the crater (Kagoshima Meteorological Office, 2014). Because the northern and central bay basins are closer to the volcano than the observatory, large amounts of ash were deposited on Kagoshima Bay during that period. The accumulation of large amounts of ash might have led to a decrease of the TOC and T-Hg concentrations in the sediment columns, accompanied by an increase of the χ values. After the period of high volcanic activity ended, the amount of ash in the sediments decreased, leading to the return of the TOC concentration to the previous levels. However, the increase in the T-Hg concentration after the end of this high volcanic activity period was slow compared with the observed TOC levels, suggesting a decline of the Hg supply into the sediments in this area. Tomiyasu et al. (2003) found that the sedimentation rate of volcanic materials in soils around Sakurajima Volcano is high during periods of

vigorous volcanic activity accompanied with a decrease in the proportion of organic matter. This finding evidences the magnitude of the ash accumulation during the periods of high volcanic activity after Taisho eruption and supports the hypothesis regarding the inverse relationship between TOC and magnetic susceptibility proposed in the present work.

X-ray images constitute an important evidence of the changes in the depositional processes product of the increase of Sakurajima volcano activity. As it was shown in section 3.1.6, X-radiograph of the core from station 7 reveals sedimentary layers that are not otherwise visible, since an area of high reflectance in the middle section can be clearly seen. This high reflectance area matches the increase of magnetic susceptibility and the decrease of TOC, and further reinforces the hypothesis of elevated volcanic activity giving rise to the movement of magnetic minerals into depositional environments and finally leading to the change in the relationship between TOC and T-Hg.

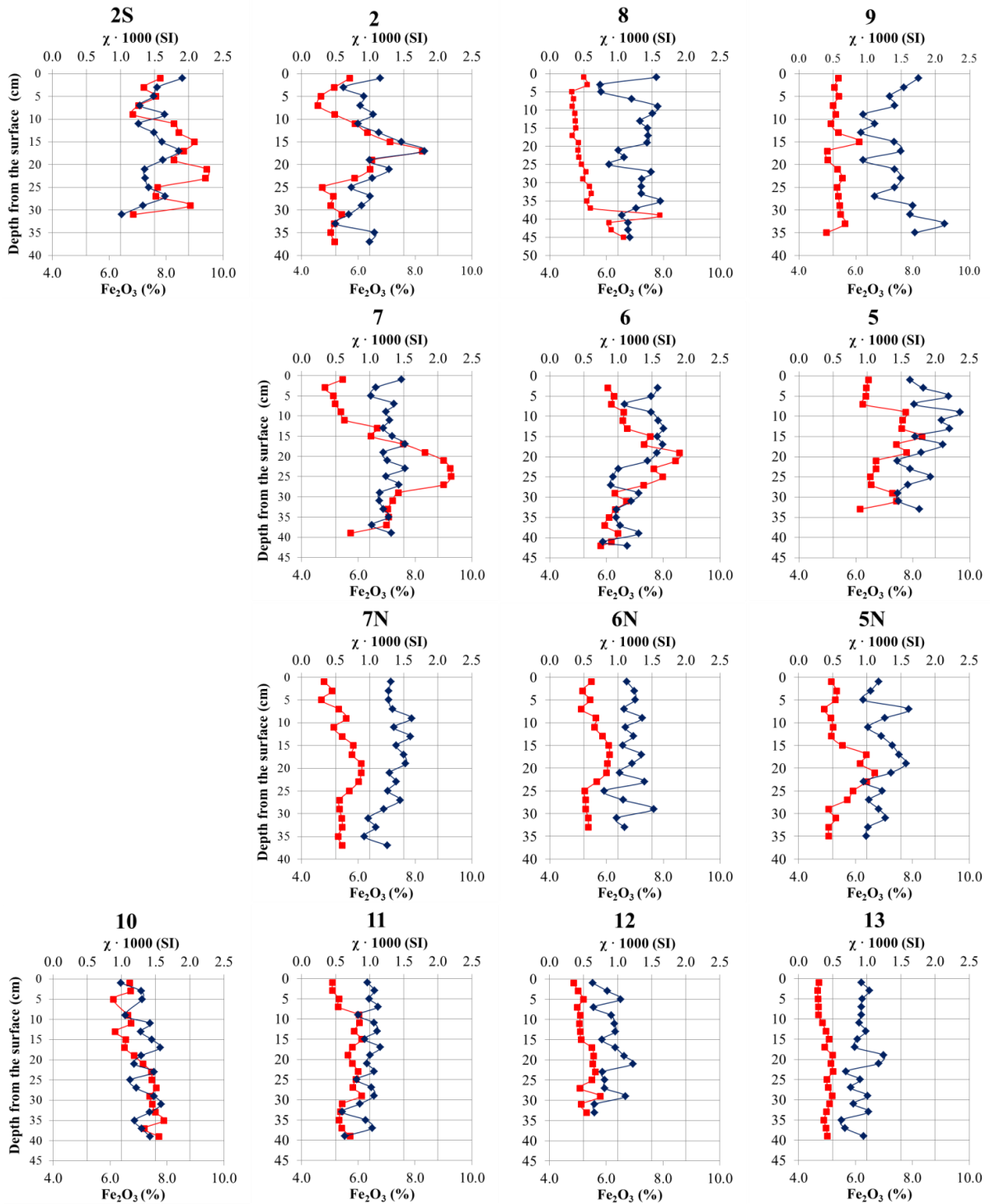


Figure 13. Vertical distribution of the magnetic susceptibility and the iron content. ■: magnetic susceptibility ($\text{SI} \times 1000$), ◆: Fe ($\text{g-Fe}_2\text{O}_3/100\text{-g}$)

In the central area (i.e., Stations 10, 11, 12 and 13), no significant correlation between T-Hg and TOC was found at any of the cores, and the mercury levels correspond to the background level of the area. The absence of correlation is probably the result of the nearly constant the vertical profiles of T-Hg, since only minor changes in the

concentration of T-Hg are observed, no correlation with any parameter can be observed. Nevertheless, when the horizontal profiles are considered, it can be observed that both organic matter and T-Hg concentration increase when moving from St. 10 to St. 13 (Figure 14). The ability of the sediments to collect Hg increases proportionally to the organic carbon content, resulting in the increase of the T-Hg levels toward station 13.

Notable findings emerge when the numerical values of the slopes of the TOC vs. T-Hg plots are evaluated. First, when the slopes obtained from the upper halves of the cores where the two linear relationships are compared (Figure 12), it can be observed that stations 5 and 5N have higher values (0.08 and 0.16, respectively) than the other stations in the area (0.03 at St. 6, 7, 6N and 7N), which provides evidence of the higher impact of fumarolic activity on the stations located closer to the fumaroles. However, the slopes at stations 6, 7, 6N and 7N are similar to the value obtained when the data from stations 10, 11, 12 and 13 are combined (Figure 14), suggesting that the impact of the hydrothermal activity on the Hg concentration in sediments from this area has decreased over time. The reason behind the decline of hydrothermal activity might be linked to the period of high volcanic activity at Sakurajima that was previously discussed. When the vertical profiles of T-Hg at the stations 7, 6, 5, 7N, 6N and 5N are observed, it can be seen how T-Hg concentration continuously decrease upwards until the middle portion of the core, then the concentration nearly stabilizes and increase slightly. This change in T-Hg concentration occurs at the same time as the profiles of TOC start increasing, after the peak in the elevated deposition of minerals of volcanic origin has been reached. The increase of the activity at Sakurajima volcano might be linked to a decrease of the hydrothermal activity at Wakamiko caldera. This is possible since Wakamiko caldera and Sakurajima volcano share the same magma chamber (Arakami, 1984).

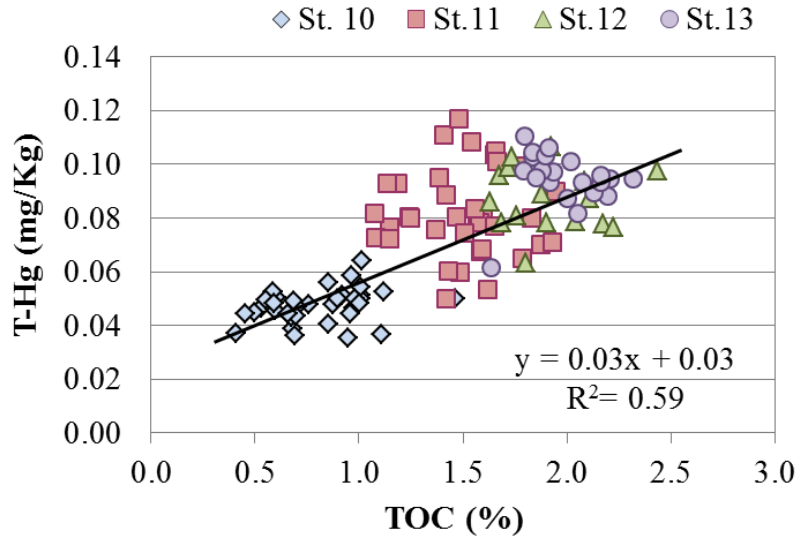


Figure 14. Correlation between T-Hg and TOC concentrations in the bottom sediments in the central area of Kagoshima Bay.

4. Conclusions

4.1. Summary

In the present study, the influence of submarine fumaroles on the spatial distribution of mercury in bottom sediments of Kagoshima Bay was studied. The distribution of toxic metals in sediments is a very complex process that depends on various parameters, for this reason the relationship between some physical and chemical factors of the sediments and the observed distribution of mercury was assessed. The physicochemical properties of the sediments change along bay by means of the influence of environmental factors: variation of the source material, which alters the amount of organic matter and particle size; volcanic activity, which incorporates ash into the sediments; and the topographical features of the bay, which affect the water exchange between the north and central basins. As a consequence of the change in the sediment properties, the distribution of mercury emitted by submarine fumaroles is affected.

Sediments from different areas of the Bay have similar chemical composition; however, variations in pH and in the concentrations of calcium and sulfur revealed how the emission of hydrothermal fluids by submarine fumaroles have a measureable effect in the surrounding environment. Topographical features of the Bay restrict the transport between the north and central areas and as a consequence, fluids released by the fumaroles do not reach the central area. For this reason, this area should be considered the background and the reference point when the impact of the fumaroles is estimated.

The horizontal distribution of mercury in the sediments showed that hydrothermal activity constitutes the principal source of Hg in Kagoshima Bay. No significant correlations were found between Hg and physicochemical parameters like particle size and elemental composition, suggesting that the distribution of Hg is not fully controlled by these variables. However, from the significant correlation between Hg and TOC profiles, the sediment organic matter content appears to have a major role in the distribution of mercury. This finding suggests that Hg emitted at Wakamiko Caldera is bound by organic matter after being in the dissolved phase.

In a zone with uniform topographical features and under similar depositional conditions, which is located to the west of the fumaroles, two distinct linear relationships between T-Hg and TOC were observed. These relationships probably result from the decrease of

the amount of Hg discharged from the submarine vents after the 1980s, which may be caused by a change of the volcanic activity at the Aira Caldera.

In the recent past, mercury released by the fumaroles was bio-accumulated by fish and constituted a potential hazard to the people living in the area. The present results indicate that the extent of the bay impacted by Hg generated from hydrothermal vents has decreased and is limited mostly to the vicinity of the emission point; this is an important finding since it suggests a decrease of the environmental risk caused by the fumaroles.

4.2. Future Studies

The present study showed that hydrothermal activity constitutes a natural source of mercury in Kagoshima Bay, that organic matter in bottom sediments is the main factor controlling mercury mobility, and that the impact of the fumaroles has decreased in recent times. This information is valuable since it helps to understand the behavior of mercury and constitutes an important step in the environmental assessment of the area. However, further experiments are needed to shed light on various topics that are worth researching in order to fully elucidate the environmental significance of mercury in this ecosystem.

It is important to understand the mechanisms by which mercury interacts with the sediments, although the present results show that organic matter controls mercury concentration; the involved species remain unclear. It is necessary to focus on operationally defined speciation analysis of mercury, which is necessary to estimate mercury speciation and its mobility. Additionally, it has been determined that organic matter is an important variable, nonetheless it is important to understand which fraction plays the most active role binding the mercury, since Total Organic Carbon represents the sum of various organic compounds which may play different roles in the distribution of mercury.

It was found that that impact from submarine fumaroles has decreased over the time, but this observation alone cannot be used to perform an integral risk assessment. For this reason, future experiments should attempt to evaluate the methylation rate and as well as to determine the levels of mercury species in sea water and marine organisms.

5. References

- Athar R, Ahmad M (2002) Heavy Metal Toxicity: Effect on plant growth and metal uptake by wheat, and on free living azotobacter. *Water, Air, and Soil Pollution* 138:165–180.
- Akagi H (1985) Analysis of methylmercury in fish and shellfish by dithizone extraction-gas chromatography. *Japanese Journal of Hygiene*. 40:293. (in Japanese)
- Akagi H, Malm O, Branches FJP, Kinjo Y, Kashima Y, Guimaraes JRD, Oliveira RB, Haraguchi K, Pfeiffer WC, Takizawa Y, Kato H (1995) Human exposure to mercury due to goldmining in the Tapajos River basin, Amazon, Brazil: speciation of mercury in human hair, blood and urine. *Water Air Soil Pollut* 80:85–94.
- Ando T, Yamamoto M, Tomiyasu T, Tsuji M, Akiba S (2010) Mercury distribution in seawater of Kagoshima Bay near the active volcano, Mt. Sakurajima in Japan. *Bull Environ Contam Toxicol* 84:477–481.
- Arakami S (1984) Formation of the Aira Caldera, Southern Kyushu, ~22,000 years ago. *J Geophys Res* 89:8485–8501.
- Araneda A, Cruces F, Torres L, Bertrand S, Fagel N, Chirinos L, Barra R, Urrutia R (2007) Changes in sub-fossil chironomid assemblages associated with volcanic sediment deposition in an Andean lake (38°S). Chile. *Rev Chil Hist Nat*. 80:41-156.
- Axelsson V (1983) The use of X-ray radiographic methods in studying sedimentary properties and rates of sediment accumulation. *Hydrobiologia* 103: 65-69.
- Carranza CU, Tomita K, Oki K, (1994) Preliminary report on the mineralogical studies of bottom surface sediments of Kagoshima Bay. *Rep Fac Sci Kagoshima Univ. (Earth Sci & Biol)* 27:23–40.
- Celo V, Lean DRS, Scott SL (2006) Abiotic methylation of mercury in the aquatic environment. *Sci Total Environ*. 368:126–137.
- Cho K, Kawaharada R, Tanaka H (1991) Sediment Load of rivers flowing into Kagoshima inner Bay and its diffusion. *Bulletin of the Faculty of Agriculture, Kagoshima University*, 41: 69-79 (In Japanese)

Debret M, Sebag D, Desmet M, Balsam W, Copard Y, Mourier B, Susperrigui A, Arnaud F, Bentaleb I, Chapron E, Lalliers-Vergès E, Winiarski T (2011) Spectrocolorimetric interpretation of sedimentary dynamics: The new “Q7/4 diagram”. *Earth-Sci. Rev.* 109:1-19.

El Bilali L, Rasmussen PE, Hall GEM, Fortin D (2002) Role of sediment composition in trace metal distribution in lake sediments. *Appl Geochem* 17:1171–1181.

European Union (2001) Decision No. 2455/2001/EC of the European Parliament and of the Council of 20 November 2001 establishing the list of priority substances in the field of water policy and amending Directive 2000/60/EC. *Official Journal of the European Communities*.

Gallego SM, Benavides MP, Tomaro ML (1996) Effect of heavy metal ion excess on sunflower leaves: Evidence for involvement of oxidative stress. *Plant Science* 121:151–159.

Guimaraes, JTF, Cohen MCL, Fanca MC, Silva AKT, Rodrigues SFS (2013) Mineralogical and geochemical influences on sediment color of Amazon wetlands analyzed by visible spectrophotometry. *Acta Amaz.* 43: 331 – 342.

Graeme KA, Pollack CV (1998) Heavy metal toxicity, part I: arsenic and mercury. *The Journal of Emergency Medicine* 16:45–56.

Hahladakis J, Smaragdaki E, Vasilaki G, Gidaracos E (2013) Use of Sediment Quality Guidelines and pollution indicators for the assessment of heavy metal and PAH contamination in Greek surficial sea and lake sediments. *Environ Monit Assess* 185:2843–2853.

Harada M (1995) Minamata disease: Methylmercury poisoning in Japan caused by environmental pollution. *Crit Rev Toxicol* 25:1–24.

Hayasaka S, Oki K, Otsuka H, Higashikawa S (1976) Geological study on Kagoshima Bay, south Kyushu, Japan. Part III - Submarine topography and bottom sediments of the Bay-head area. *Rep Fac Sci Kagoshima Univ (Math., Phys. & Chem.)* 9: 53–73. (In Japanese).

Hunerlach MP, Alpers CN, Marvin-DiPasquale M, Taylor HE, De Wild JF (2004) Geochemistry of mercury and other trace elements in fluvial tailings upstream of

Daguerre Point Dam, Yuba River, California, August 2001: U.S. Geological Survey Scientific Investigations Report 2004-5165, 66.

Hurvich, L.M., Jameson, D., 1957. An opponent-process theory of color vision. *Psychological review*. 64(6), 384-404.

Kagoshima Prefecture (1975) Environmental Report of Environmental Survey of Mercury Pollution in Kagoshima Bay. (In Japanese).

Kagoshima Prefecture (2008) Environmental Health Center Report Volume 9. 2008. <https://www.pref.kagoshima.jp/ad08/kurashi-kankyo/kankyo/kankyohoken/shoho/documents/siryo9-1.pdf> Accessed 15 December 2014. (In Japanese).

Kagoshima Meteorological Office. Monthly count of Sakurajima volcano eruptions. http://www.jma-net.go.jp/kagoshima/vol/data/skr_exp_num.html. Accessed 3 December 2014. (In Japanese).

Keating, M. H., 1997. Mercury study report to congress, Volume 1: Executive summary. United States Environmental Protection Agency.

Kim E, Noh S, Lee YG, Kundu SR, Lee BG, Park K, Han S (2014) Mercury and methylmercury flux estimation and sediment distribution in an industrialized urban bay. *Mar Chem* 158:59–68.

Kono Y, Tomiyasu T (2014) Variations in atmospheric mercury concentration in Kagoshima City during 2010-2012. *Bunseki Kagaku* 63:17–21. (In Japanese)

Liu M, Yang Y, Yun X, Zhang M, Li QX, Wang L (2014) Distribution and ecological assessment of heavy metals in surface sediments of the East Lake, China. *Ecotoxicology* 23:92–101.

Lopez P, Navarro R, Marce R, Ordoñez J, Caputo L, Armengol J, (2006) Elemental Ratios in sediments as indicators of ecological processes in Spanish reservoirs. *Limnetica*, 25: 499-512.

Malm O, Branches FJP, Akagi H, Castro MB, Pfeiffer WC, Harada M, Bastos WR, Kato H (1995) Mercury and methylmercury in fish and human hair from the Tapajos river basin, Brazil. *Sci Total Environ* 175:141–150.

Merritt KA, Amirbahman A (2009) Mercury methylation dynamics in estuarine and coastal marine environments - A Critical Review. *Earth-Sci Rev* 96: 54–66.

Ministry of environment, Japan (2004) Determination by the wet digestion/reduction/cold vapor atomic absorption spectrometry (CVAAS) (circulation-open air flow system). In: *Mercury Analysis Manual*, pp 23–24.

Miyamoto J, Kono Y, Tomiyasu T, Imura R (2008) Measurement of mercury contents in *parmotrema tinctorum* (parmeliaceae) around Sakurajima Volcano, Kagoshima, Japan. *Lichenology* 7:143–151.

Mix AC, Rugh W, Pias NG, Viers S Leg 138 Shipboard Sedimentologists and Leg 138 Scientific Party (1992) Color reflectance spectroscopy: A tool for rapid characterization of deep-sea sediments. *Proc. ODP Init. Rep.* 138, 67–78.

More F, Kraepiel A, Amyot M (1998) The Chemical Cycle and Bioaccumulation of Mercury. *Annu. Rev. Ecol. Syst.* 29:543–66.

Nagase I, Ose Y, Sato T, Ishikawa T (1984) Mercury methylation by compounds in humic material. *Sci Total Environ* 32:147–156. doi: 10.1016/0048-9697(84)90127-X

Oki K (1989) Ecological analysis of benthonic foraminifera in Kagoshima Bay, South Kyushu, Japan. *South Pacific Study* 10:1–191.

Osaka J, Hirabayashi T, Ozawa T, Onishi H, Sakamoto J (1976) Study of Submarine Volcanic Activity in the Northern Area of Sakurajima. Ministry of Education, Science and Culture. Coordinated Research Survey Report, pp 48–63 (In Japanese).

Pacyna EG, Pacyna JM, Sundseth, K, Munthe J, Kindbom K, Wilson S, Steenhuisen F, Maxson P (2010) Global emission of mercury to the atmosphere from anthropogenic sources in 2005 and projections to 2020. *Atmos Environ* 44:2487–2499.

Pyle DM, Mather TA (2003) The importance of volcanic emissions for the global atmospheric mercury cycle. *Atmos. Environ.* 37:5115–5124.

Sakamoto H (1985) The Distribution of Mercury, Arsenic and Antimonium in Sediments of Kagoshima Bay. *Bull Chem Soc Jpn* 58:580–587.

Sakamoto H, Takashi T, Yonehara N (1993) Mercury Content and its Distribution in Sea Water of Kagoshima Bay. Rep Fac Sci Kagoshima Univ (Math Phys & Chem) 26:75–91.

Sakamoto, H, Tomiyasu T, Yonehara N (1995) The contents and chemical forms of mercury in sediments from Kagoshima Bay, in comparison with Minamata Bay and Yatsushiro Sea, southwestern Japan. *Geochem J* 29:97–105.

Sunderland EM, Gobas FAPC, Branfireun BA, Heyes A (2006) Environmental controls on the speciation and distribution of mercury in coastal sediments. *Mar Chem* 102:111–123.

Sweet L, Zelikoff T (2001) Toxicology and Immunotoxicology of Mercury: A Comparative Review In Fish And Humans. *Journal of Toxicology and Environmental Health, Part B*, 4:161–205.

Tomiyasu T, Nagano A, Sakamoto H, Yonehara N (2000) Background levels of atmospheric mercury in Kagoshima City, and influence of mercury emission from Sakurajima Volcano, Southern Kyushu, Japan. *Sci Tot Environ* 259:231–237.

Tomiyasu, T. Okada, M. Imura, R. Sakamoto, H (2003) Vertical variations in the concentration of mercury in soils around Sakurajima Volcano, Southern Kyushu, Japan. *The Science of the Total Environment* 304:221-230

Tomiyasu T, Eguchi M, Sakamoto H, Anazawa K, Imura R (2006) Seasonal change and vertical movement of atmospheric mercury at Kagoshima city in relation with Sakurajima Volcano, Japan. *Geochem J* 40:253–263

Tomiyasu T, Eguchi T, Yamamoto M, Anazawa K, Sakamoto H, Ando T, Nedachi M, Marumo K (2007) Influence of submarine fumaroles on the distribution of mercury in the sediment of Kagoshima Bay, Japan. *Mar Chem* 107:173–183.

Tsutsumi K, Kohno J, Anraku K, Kikukawa, H, Shimozono K, Kinoshita K (2009) Study of River Water Expansion in the Inner Kagoshima Bay by the Infrared Remote Sensing. *Journal of the Remote Sensing Society of Japan* 19: 37-49. (In Japanese).

Tucker ME (2003) Sedimentary rocks in the field. Wiley-Interscience 3rd ed, New York, 244 p.

United Nations Environment Programme (2013) Global Mercury Assessment 2013: Sources, Emissions, Releases and Environmental Transport. UNEP Chemicals Branch, Geneva, Switzerland.

Varekamp JC, Buseck PR (1986) Global mercury flux from volcanic and geothermal sources. *Appl Geochem* 1:65–73.

Whalin LE, Mason KR (2007) Factors influencing the oxidation, reduction, methylation and demethylation of mercury species in coastal waters. *Mar Chem* 7:278–294.

World Health Organization. (2000) Mercury. In: *Air Quality Guidelines for Europe*, 2nd edn. WHO Regional Office for Europe, Copenhagen pp 157–161.

Xu W, Yan W, Huang W, Chen Z, Wang S, Miao L, Zhong L, Chen H (2013) Mercury profiles in surface sediments from ten bays along the coast of Southern China. *Mar Poll Bull* 76:394–399.